UNIVERSIDAD DE INVESTIGACIÓN DE TECNOLOGÍA EXPERIMENTAL YACHAY

Escuela de Ciencias Químicas e Ingeniería

Silicon carbide production from biomass

Trabajo de integración curricular presentado como requisito para la obtención del título de Ingeniero en Polímeros

Autora:

Rudy Riera

Tutora:

Ph.D. Alicia Sommer

Urcuquí, marzo del 2025

Autoría

Yo, **Rudy Riera**, con cédula de identidad 0704935071, declaro que las ideas, juicios, valoraciones, interpretaciones, consultas bibliográficas, definiciones y conceptualizaciones expuestas en el presente trabajo; así cómo, los procedimientos y herramientas utilizadas en la investigación, son de absoluta responsabilidad de el/la autor/a del trabajo de integración curricular. Así mismo, me acojo a los reglamentos internos de la Universidad de Investigación de Tecnología Experimental Yachay.

Urcuquí, marzo del 2025.

_____

Rudy Riera

CI: 0704935071

Autorización de publicación

Yo, **Rudy Riera**, con cédula de identidad 0704935071, cedo a la Universidad de Investigación de Tecnología Experimental Yachay, los derechos de publicación de la presente obra, sin que deba haber un reconocimiento económico por este concepto. Declaro además que el texto del presente trabajo de titulación no podrá ser cedido a ninguna empresa editorial para su publicación u otros fines, sin contar previamente con la autorización escrita de la Universidad.

Asimismo, autorizo a la Universidad que realice la digitalización y publicación de este trabajo de integración curricular en el repositorio virtual, de conformidad a lo dispuesto en el Art. 144 de la Ley Orgánica de Educación

Urcuquí, marzo del 2025.

_____

Rudy Riera

CI: 0704935071

Dedication

To my family.

Rudy Riera

Acknowledgment

My deepest gratitude to all the people that made the completion of this work possible.

Rudy Riera

Resumen

Se sintetizó carburo de silicio a partir de residuos agrícolas, semilla de aguacate sin almidón y aceite de cocina reciclado, como materia prima, y dopado con Zn/Co (II) o Pd (II). El material fue sintetizado vía el método HIPE (Emulsión de Alta Fase Interna) seguido de un proceso de pirólisis en un horno de tubo a 900 °C por un período de 6 horas con una rampa de calentamiento de 1 °C/min. Los materiales resultantes fueron caracterizados por ATR-FTIR (Espectroscopía Infrarroja por Transformada de Fourier con Reflexión Total Atenuada), XRD (Difracción de Rayos-X), XPS (Espectroscopía de Fotoelectrones de Rayos-X) y XRF (Fluorescencia de Rayos-X). El material resultante fue una mezcla entre sílice y carburo de silicio mecánicamente frágil, con un aspecto brillante en la capa externa y un color opaco en las capas más internas. Las mejores muestras, con respecto a contenido de carburo de silicio, fueron las sintetizadas con el mayor contenido de semilla de aguacate. Los monolitos fueron exitosamente funcionalizados con los metales respectivos y fueron probados como adsorbentes y catalizadores en la adsorción de Cr(VI) y la foto-reducción del 4 nitrofenol (4-NP), respectivamente. Los monolitos funcionalizados con metales mostraron mejor capacidad de adsorción de Cr(VI). Así mismo, los monolitos con metales mejoraron la estabilidad en la reacción de foto-reducción de 4-NP en presencia de un agente reductor fuerte, con lo cual se pueden conducir estudios adicionales para determinar su viabilidad en la producción de hidrógeno.

Palabras Clave: carburo de silicio, HIPEs, adsorbentes, producción de hidrógeno, biomasa, paladio.

Abstract

Silicon carbide was synthesized from agricultural residues, starch-less avocado seed and recycled cooking oil, as raw materials and doped with Zn/Co (II) or Pd (II). The material was synthesized via the HIPE (High Internal Phase Emulsion) method, followed by a pyrolysis process in the tube furnace at 900 °C for 6 hours with a heating rate of 1 °C/min. The resulting material was characterized by ATR-FTIR (Attenuated Total Reflectance Fourier Transform Infrared Spectroscopy), XRD (X-Ray Powder Diffraction), XPS (X-Ray Photoelectron Spectroscopy) and XRF (X-Ray Fluorescence). The material obtained was a mixture of silica and silicon carbide, mechanically fragile and with a shining outer layer and an opaque color in the inside layers. The best samples with respect to silicon carbide content were the ones synthesized with the highest content of avocado seed. The monoliths were successfully functionalized with the respective metals and were tested as adsorbents and catalysts in the adsorption of Cr(VI) and the photoreduction of 4-nitrophenol (4-NP). The metal-functionalized monoliths showed a better Cr(VI) adsorption capacity. Likewise, the metal-containing monoliths enhanced the photoreduction of 4-NP in the presence of a strong reducing agent, with which additional research can be conducted in order to determine their feasibility in hydrogen production.

Keywords: silicon carbide, HIPEs, adsorbents, hydrogen production, palladium.

Contents

List of Tables

List of Figures

Chapter 1

Introduction

The tendency of focusing research in the development of environmentally sustainable materials and the harnessing of agricultural waste products is ever increasing [2]. In particular, it has prompted the usage of alternative carbon sources for the production of advanced materials for various applications. The synthesis of hierarchically porous silicon carbide from different underemployed waste products, introduces an opportunity for material development in a sustainable manner [3]. The material produced (silicon carbide) displays distinctive structural and chemical properties, rendering it fitting for diverse applications such as water remediation, catalysis and energy storage [4]. This thesis focuses on the production of hierarchically porous silicon carbide from avocado seed and recycled cooking oil as environmentally-friendly sources of carbon, with the main objective of giving an added value to this ceramic material with prospective applications in metal adsorption and hydrogen production. The study is centered on the effective synthesis of silicon carbide, its subsequent characterization, and evaluation of its performance in the applications aforementioned.

1.1 Problem statement

The majority of industries generate tons of waste, in both solid and liquid form, which can represent an environmental burden if not appropriately treated [5]. These volumes of waste have the potential to be repurposed as materials with an added value [6]. In particular, the oil industry generates a significant amount of waste in the form of seeds, peels, seed husks and pulp that are usually discarded or employed for low-value applications [7]. Ecuador as

a country, is a producer of avocado that satisfies the national demand; however it does not excel in avocado and avocado derived products exports [8]. Nonetheless, the production of avocado crops and derived products is still a significant producer of organic waste; therefore, the avocado oil industry presents a great opportunity for taking advantage of this agroindustrial waste and transforming it into higher-value materials, namely, as a carbon source for the synthesis of silicon carbide that can be employed in applications such as sorption, catalysis and electrochemistry [9]. Additionally, recycled cooking oil represents yet another form of waste repurposing and an additional source of carbon. It is worth noting that the avocado seed source was the starch-less remnants of a CEDIA-funded previous project ("Hacia un modelo sistémico para la creación de emprendimientos de base científico – tecnológico en las instituciones de educación superior del Ecuador"), which further serves the goal of repurposing material.

Particularly, the synthesis of hierarchically porous silicon carbide structures is of great interest as it can further provide a special structure for sorption and catalysis applications [9]. In this manner, this thesis focuses on the synthesis of porous silicon carbide from avocado seed and recycled cooking oil as renewable and sustainable sources of carbon, for the production of added value materials with potential applications in industries such as energy, environmental remediation, and catalysis.

1.2 Objectives

1.2.1 General Objective

To develop an efficient method for the synthesis of hierarchically porous silicon carbide materials using avocado seed waste and recycled oil.

1.2.2 Specific Objectives

- To employ the HIPE (High Internal Phase Emulsion) method and pyrolysis for the synthesis process of porous silicon carbide from avocado seed and recycled oil as carbon source.

- To characterize the physico-chemical properties of the material obtained, using tech-

niques such as XRD (X-ray Diffraction), XPS (X-ray Photoelectron Spectroscopy), XRF (X-ray fluorescence), AAS (Atomic Absorption Spectroscopy) and FTIR (Fourier Transform Infrared Spectroscopy).

- To explore the use of silicon carbide as an adsorbent for environmental remediation applications, with a focal point on the capability to remove polluting elements, such as chromium, in water.

- To examine the possible applications of the porous silicon carbide in hydrogen production as an alternative source of energy.

Chapter 2

Theoretical Background

2.1 Silicon carbide

Silicon carbide or carborundum (SiC) is a ceramic material that consists of the interlocking of sheets of silicon and carbon that are covalently bound together. SiC is composed of a tetravalent element (carbon) that is connected to a semiconductor element (silicon). Three silicon atoms are linked to a carbon atom inside the double layer and linked to a silicon atom below it forming a strong tetrahedral structure with sp^3-hybridized bonds, which confer outstanding chemical and thermal stability. The distance that separates adjacent silicon from carbon atoms is about 3.08 Å among all types of crystallographic structures. Likewise, the distance that separates silicon and carbon atoms from each other is around 1.89 Å for all Si-C bonds [10–13]. The crystallographic structures of SiC comprises closely packed bi-layers of silicon and carbon atoms; different structures, denominated polytypes, arise from the formation of different stacking sequences of said bi-layers [10–13]. Considering the first double layer in the sequence as position A, the following double layer as position B or C, the different polytypes can be obtained by permuting these positions [12]. SiC has numerous polytypes, however it is usual to refer to 3C-SiC as β-SiC and the non-cubic structures (4H-SiC, 6H-SiC, 9R-SiC, and 15R-SiC) as α-SiC. Additionally, the former are categorized as low temperature polytypes as the nucleation and growth processes require lower temperatures than those of α-SiC. There around 250 polytypes of SiC from which the most common ones are cubic 3C, hexagonal 4H and 6H, and rhombohedral R and depending on the polytype of SiC, different optical, electrical and thermal properties can

be tailored upon the material [11, 13].

Silicon carbide has interesting properties such as high breakdown electric field, high thermal conductivity, good chemical inertness, high hardness, high electron drift velocity, low thermal expansion coefficient, wear resistance, high strength, oxidation resistance as well as remarkable thermal, chemical and mechanical stability [10–16]. Since SiC has a wide bandgap refractory (2.39 eV for 3C-SiC, 3.02 eV for 6H-SiC), the material is able to be used for semiconductor devices showing efficient functionality even at high temperatures up to 600 °C [12]. SiC is also capable of harvesting light in the visible light and ultraviolet spectrum [15], making it suitable for applications such as high power electronics, photonic devices, catalyst supports in harsh environments, sensors, quantum computing, functional ceramics, composites and heterogeneous catalyst supports [12–14, 16].

Amongst SiC's physical and mechanical properties, it can be noted that it shows a hardness of approximately 46 GPa; a Mohs hardness that measures at 9.2; modulus of elasticity of 425 GPa; coefficient of friction of 0.16; Vickers microdensity hardness that ranges from 3000 to 3300 kg mm^{-2} and Knoop hardness between 2670 and 2815 kg mm^{-2}. This material sublimates at around 2700 °C instead of melting and forms a strong surface film of silicon dioxide when exposed to heat in the presence of air; the latter causing its resistance to oxidation up to 1850 °C and 1500 °C for short and long periods of time respectively [12–14, 16]. In terms of other chemical properties, silicon carbide exhibits good chemical resistance and oxidation resistance amid various alloys and chemical compounds that are heat-resistant. This material shows significant oxidation above 800 °C by concentrated acids and overall high chemical conditions compared to amorphous ceramics with more limited thermal stability. All of these assets and applications represent an important challenge for researchers to further investigate and develop approaches that are economically feasible and effective for the synthesis of silicon carbide-based materials [12]. In particular, silicon carbide-based nanomaterials are of great interest among researchers due to the higher surface area of SiC nanoparticles when compared to its bulk counterparts. Moreover, such characteristics impact their homogeneity, chemical stability and overall applications, such as the production of stable colloidal solutions and ceramic slurries [11].

2.2 Synthesis of silicon carbide

Silicon carbide can be scarcely found in nature in the form of moissanite; it was discovered as a component analyzed within a meteorite in Arizona in 1905 by Dr. Ferdinand Henri Moissan. This material is vastly found outside the planet in the form of stardust among stars that are rich in carbon [17]. Owing to the fact that silicon carbide rarely occurs in nature, the synthesized version of the material is employed. Edward Goodrich Acheson pioneered the commercial synthesis of SiC in 1892 by creating diamonds from clay and powdered coke which are rich in aluminum silicate and carbon respectively. The outcome exhibited crystals denoted as carborundum due to its similar hardness to that of corundum. The process was later patented and, although it had a synthesis temperature of about 2500 °C, it was one of the most prominent synthesis methods for production of silicon carbide [17]. Several routes have been employed to synthesize mesoporous SiC including sol–gel, direct reaction of silicon and carbon, hydrothermal acid leaching, carbothermal reduction of silica, microwave sintering, pyrolysis, pyrohydrolysis, siliconizing, thermal evaporation, sputtering, Chemical Vapor Deposition (CVD) among others [11, 12]. Amongst the most common techniques are the sol-gel technique, the carbothermal reduction method and the pyrolysis technique. For instance, the sol-gel technique was employed by [18] in the synthesis of SiC nanopowder. TEOS, which is high in silicon content, was employed along Resol, which is high in carbon content, and hydrochloric acid as a catalyst agent by being hydrolysed and gelated in mixture [11, 12]. β-SiC nanoparticles with high surface area and large particle size were obtained as a result. Moreover, pH was found to be a factor in the stabilization of the solution with higher pH values giving a less stable solution [18].

Another example is the method presented by [19] for synthesizing SiC from solid residue, as carbon source, and sandstone powder, as the silicon source. The materials were sintered at temperatures in the range of 1300 and 1600 °C in an argon atmosphere resulting in the production of SiC whiskers and SiC particulates. Rajarao et al. used a similar approach for the synthesis of porous β-SiC nanoparticles with particle size in the range of 20–80 nm employing using waste macadamia shells as the carbon source alongside silica at the relatively low synthesis temperature of 800 °C in an inert atmosphere [11]. A different synthesis method was utilized in the creation of highly crystallized SiC whiskers from calcining tis-

sue and glass microspheres at high temperatures, which proved to enhance the crystallinity and lack of impurities of the yielded materials when compared to lower temperatures. In another study, an approach was devised to employ printed circuit boards as a source of both silicon and carbon for the development of SiC nanoparticles. Furthermore, an alternating current multi-arc plasma device was created for the synthesis of SiC nanoparticles with particle size of 7-10 nm by a reaction of decomposition of triethylsilane [12].

Lee and Cutler developed a method for synthesizing silicon carbide based on biomass utilizing rice husk as the main source [20]. The "green"- or plant-based precursors of carbon that come from waste biomass are a great alternative as carbon sources for the synthesis of silicon carbide. Among the studies carried out with biomass-based silicon carbide, many crop residues and cereal straws are used [21]. Many studies have employed rice husks to develop silicon carbide nanoparticles. Rice husks as a by-product are usually disposed via soil burning or calcination processes; however, it can be given added value by leveraging its potential due its lignin, cellulose and hydrated silica content. Su et al. synthesized silicon carbide nanoparticles by magnesiothermic reduction using rice husks and operational temperature of 600 °C. The rice husk and magnesium were mixed in the form of powders, reduced in a furnace in an inert atmosphere and, as a result, green powder β-SiC nanoparticles were obtained [21].

Other examples of carbon precursors are: barley husk, wheat, macadamia shells, corn cobs, etc [3, 11, 22]. Studies such as that of [3] showcases an effective approach to use sandstone and corn cobs to create nanoporous β-SiC via carbothermal reduction, which is an eco-friendly alternative to conventional SiC synthesis as well as added value to agricultural waste materials [3, 11, 22]. All of these are high in cellulose from which carbon can be obtained, as well as a moderate amount of silica, from the outer epidermis when it is assimilated during the regeneration of the cell wall. Besides, their great potential also relies on the accessibility, availability and low costs of these materials [10].

Furthermore, as the synthesis of silicon carbide requires a source of carbon, the present project proposes the usage of an additional source through the employment of recycled cooking oil as the oil phase of the emulsion process that is to be used for the preparation of the monoliths. This is proposed with the objective of ensuring the formation of silicon carbide and adding value to an otherwise wasted product.

2.3 Applications of SiC

Since 1994, when SiC nanorods were first synthesized, many advances have been made in the synthesis of SiC-based nanomaterials. The latter can be classified according to morphology dimension in 0D, e.g. nanocrystals; 1D, e.g. nanorods; 2D, e.g. nanofilms; and 3D, e.g. bulk SiC materials or SiC-based composites. Among the applications that these structures can have are: optoelectronics (for 0D), applications in mesoscopic physics and nanometric scale devices (for 1D), applications in light emitters, sensors, solar cells (for 2D), and energy conversion and storage applications (for 3D) [23]. Owing to its biological and chemical inertness, resistance to oxidation and corrosion by body fluids, flexibility, moldability, high hardness, bio-compatibility and adaptability, silicon carbide has been used in the biomedical industry [11, 23]. SiC as a biomaterial has been used both in-vitro and in-vivo in biomedical applications such as: hip implants and hip replacements, ortho implants, artificial heart valves and prosthetic bone replacements; furthermore, SiC is also apt for biosensing, due to its capability to prevent electron-hole pairs, generated across the bandgap due to activation, from recombining [11, 24]. For instance, silicon nanoparticles have been employed in detection of superoxide in superoxide dismutase in conditions of brief periods of time and low detection limit [23]. Other related applications, such as lab-on-chip, medical devices, RNA purification, dental implants, cell imaging, DNA transformation, DNA sensing, etc., have implied the usage of SiC [11, 23, 24]. SiC is an outstanding technology for high power electronics, especially in high temperature conditions due to its wide bandgap and thermal stability [13]. These materials exhibit significant advantages over other electronic components, namely a high power rating and lower switching losses, tolerance to harsh thermal conditions, lower leakage current of the junctions and higher efficiency. Theoretically, the junction temperature of SiC-based devices is at 600 °C and the range of operating temperature is between 200-300 °C [25]. SiC diodes are apt for operation at high ratings of current density and lower size of cooling systems, compared to its Si counterparts. Electric vehicles, systems of renewable energy, sensors, detectors, aircraft and other aerospace applications are some of the devices that benefit from this technology [25]. SiC is also a rising technology for photonics integrated circuits (PICs) and quantum photonic integrated circuits (QPICs). When compared to

other semiconductors, the mature growth and processing of SiC for power electronics is greater for photonic devices. SiC as a wide band gap material highly resistant to radiation is appealing as a solid medium for detection of radiation. The nuclear and subnuclear applications that require these sorts of materials leverage on their radiation hardness as the high fluxes of radiation are extremely damaging to the performance of the detectors [26]. Silicon carbide is usually combined with other compounds such as boron and carbon in order to enhance properties such as creep resistance [23]. Similarly, natural resources such as plants are used to modify its physical and chemical properties; namely stiffness, flexibility, abrasion resistance and other mechanical properties; for potential biomedical and biological applications [11].

SiC is also used in membrane technology for applications such as wastewater treatment. Wastewater pollutes both water and soil and this ongoing issue is present in a variety of industries [11, 24]. There have been many approaches to solve this problem, namely sedimentation, separation by gravity, flocculation, skimming, among others. These techniques can be of physical or chemical nature, nonetheless, they have some limitations in common, such as low economical feasibility, high sludge generation and relatively low efficiency [23]. In comparison, ceramic membranes employ techniques such as ultra-, macro- and nano- filtration for the treatment of wastewater, conferring a better efficiency and an intermediate energetic cost [23]. The main disadvantage to this method is fouling; however, this effect can be minimized by fouling reduction hydrophilicity, which is achieved through coating with nonpolar tides; hence, the creation of silicon carbide ultra-filtration hydrophilic membranes, which depict lower degrees of fouling, homogeneity of pore size, good porosity, high fluxes and a large lifespan [23]. Nonetheless, silicon carbide as a bulk material presents advantages over nanomaterial structures due to factors such as separation of the pollutant from the material and scalability.

The chemical stability, high surface area and porous structure of silicon carbide confer this material the suitability for Cr(VI) adsorption [27]. Chromium(VI) is a toxic and carcinogenic heavy metal that is a significant pollutant in water bodies [28, 29]. Not only is this an environmental issue but an economic and health issue that threatens all living beings. The presence of such components in the industries of wood preservation, textile dyes, leather tannings, electroplating, among others, represents a high risk [29]. On that

account, the removal of this metal from aqueos solutions is of great significance and can be performed through the usage of porous structure of silicon carbide.

2.4 Hierarchically Porous Materials

The general definition of hierarchically porous materials is materials whose composition contains organized structural pores on various length scales. This involves three different length pores, among which there are micro- (<2 nm), meso- (2-50 nm) and macroscopic (>50 nm) pores [30]. However there are many kinds of classification of hierarchical porosity that can be found in the literature such as: according their availability to an external fluid (IUPAC) there are open and close pores, pore shape (cylindrical, ink bottle shaped or funnel shaped) and roughness surface with depth and width of pore. Hierarchical porous materials are employed to obtain excellent structures for novel application materials in the fields of catalysis, sorption, separation, energy storage and conversion, sensing and biomedicine [31].

In the last decade, numerous investigations have focused on the fabrication of hierarchically porous materials. There are many methods such as: the dual surfactant templating, colloidal crystal templating, polymer templating, bioinspiring process, emulsion templating, freeze-drying, phase separation, selective leaching, replication, zeolithization, sol-gel controlling and post treatment [31]. Depending on the research to be carried out, these methods can be classified as follows: combining chemical and physical supplementary methods or on the bases of introducing macro-porous templates in the reaction media together with small scale templates. Furthermore, a synthesis strategy has been developed based on the self-formation phenomenon which takes advantage of the chemistry of the metal alkoxides and metal alkyls to produce a porous hierarchy without the use of external templates. In the same way this process involves only procedures based on chemical processes such as phase separation, zeolithization, self-formation phenomenon and emulsion templating, high internal phase emulsion (HIPE) [32], from which the latter is of interest in the present work.

2.5 High Internal Phase Emulsions (HIPEs)

High Internal Phase Emulsion or HIPE is a method that consists of the production of hierarchically structured porous monoliths that present a controlled shape and pore size [33]. The HIPE method is characterized by an internal phase volume fraction, which indicates the maximum volume that spheres can achieve when effectively and densely packed within a stated space, that exceeds the packing limit (over 74%) which determines under certain conditions the droplets may adopt polygonal shapes due to them being tightly packed together [30, 34]. HIPEs are involved in the application of hierarchically porous monolithic materials, such as silica monoliths, with a high level of porosity that can be attributed to the great magnitude of interconnection between the pores [35]. The homogenization conditions and composition of HIPEs are strongly related to the dimensions of the droplets within their matrix and typically the droplet size decreases when the homogenization time increases and increasing surfactant concentration [35, 36]. HIPEs as all emulsions, which are mixtures of immiscible solutions that consists of a droplet phase dispersed in a matrix or continuous phase, can be classified as water-in-oil (W/O) or oil-in-water (O/W) types in function on the polarities of the external and internal phase. The former emulsion is formed when an aqueous solution is dispersed in the form of droplets in an organic solvent, and the latter is the opposite. In order to create an emulsion, a surfactant is needed to combine the immiscible fluids; this substance, known as emulsifier, serves to promote the stabilization of the fluids [30, 36]. The stabilization of these types of emulsions is a key step in the development of hierarchical porous materials in view of the fact that it prevents the separation or inversion of phases. For this matter, surfactants are the most employed because of their capability to stabilize effectively in various types of emulsions. Surfactants such as detergents and emulsifiers help lower the surface tension between the immiscible liquids that form an emulsion [37]. Commercially, these surfactants are known as poloxamers or Pluronics, which are a group of triblock copolymers formed by amphiphilic polypropylene oxide (PPO) and hydrophilic polyethylene oxide (PEO) $((PEO)_m - (PPO)_n - (PEO)_m)$. The different types of Pluronics available are a result of the change in relative composition of those main blocks in order to adjust the hydrophilic–lipophilic balance (HLB), that is, adjusting the structure. Additionally, these surfactants are applied in the pharmaceuti-

cal, food, and cosmetic industries because of their non-toxic, dispersant, solubilization and emulsifying properties [38, 39]. Pluronic® P123 ($PEO_{20} - PPO_{70} - PEO_{20}$) is one of the most commonly used polymeric. It is worth noting that the Pluronics employ a name code that starts with a letter L (liquid), P (paste) and F (flake) that indicates the physical state of the compound at room temperature. Subsequently, there are two or three digits, from which the first one or two represent the molar mass of the PPO when multiplied by 300; likewise, the last number reflects the amount in percentage of PEO when multiplied by 10. The hydrophilic part of the linear structure has great affinity with water owing to its capability to form hydrogen bonds with molecules of water. Meanwhile, the hydrophobic segments of PPO of the structure link to nonpolar components. The amphiphilic character of this compound is what allows it to form micelles that are composed of a hydrophobic core and hydrophilic outer shell. These micelles can be exhibited in hexagonal, spherical or tubular forms [39–41]. Originally the HIPE method was devised by Backov et al. in 2009 [33]; the research team employed a molecular surfactant as an stabilizing agent for the direct stabilization of O/W high internal phase emulsion. Subsequently, the oil droplets serve as a template to develop macropores in the sol-gel method; analogously the surfactant micelles induce the formation of mesopores. The templates applied are then removed in order to release the porosity; this is done by solvent extraction or by calcination. Therefore, with this approach, a dual template structure can be obtained: a direct emulsion at the macroscopic level and micellar templates at the mesoscopic level [37]. Furthermore, based on the arrangement of pore sizes, multilevel porous compositions provide exceptional properties upon materials. For example, the combination of micropores and mesopores results in large surface areas and pore volumes, which in turn, confers tailoring of size and shape of pores. Meanwhile, the use of macropores implies the reduction of transport limitations and eases the mass transport to the active sites upon materials [30].

2.6   Preparation of HIPEs

There are many methods for the preparation of HIPEs; amongst them there are: the one–step method, which is the most common and consists of using an emulsifier usually dissolved or dispersed in the continuous phase prior to homogenization and blending oil and

water. The two-step method can be used to reduce the size of the droplets within HIPEs, in this case it is necessary to use a high-shear mixer to blend water and oil. Another method is the phase inversion method, which involves the conversion of an O/W into W/O or viceversa; for this method it is necessary to tune the oil water/oil ratio, pH, ionic strength, temperature or surfactant type [36]. Finally, the last technique is the mold curing method, the HIPEs can be used as templates to form porous materials with adjustable pore size and morphologies, also an organic solvent is usually employed as the oil phase and a gelling polymer is dissolved in the aqueous phase [36]. The research group of Backov et al. [33] conducted the synthesis of a high internal phase emulsion of oil-in-water. The system involved a silica precursor, tetraethyl-orthosilicate (TEOS), water as the aqueous phase, dodecane as the oil phase and tetradecyltrimethylammonium bromide (TTAB) as the surfactant or stabilizing agent. The study yielded a material with macro/mesoporous structure with an average mesoporosity and high specific surface area of 800 m^2g^{-1}.

The results were contrasted with the monoliths of change pH in order to analyze the impact of the latter in the structure of the monoliths, which resulted to be a highly influential factor. Additionally, Backov's team suggested that the oil volume fraction is another important influential factor in the resulting texture of the monoliths [33]. Sommer et al. [42] followed an analogous "nearly one-pot" approach for the synthesis of silica monoliths functionalized with particles of metal hexacyanoferrate (MHCF). The materials employed included TEOS for the silica precursor, cyclohexane as the oil phase and Pluronic P123 as the surfactant. The selection of the oil phase and the surfactant is due to the volatile nature of cyclohexane and biocompatibility and non-toxicity of Pluronic P123. After a calcination step and prior to the impregnation with MHCF, the outcome yielded silica monoliths with macro- and meso porosity and high specific surface area (571 m^2g^{-1}).

Thereby, this method of preparation was decided to be employed for the preparation of SiC to confer the desired porosity employing biomass residues and recycled cooking oil.

2.7 Biomass residues

2.7.1 Avocado seed

The organic waste produced from the avocado fruit lies mainly in the seeds, peels, pulp and rotten fruit that are produced in all its processing industries. These byproducts are usually disposed as animal feedstock, with a low nutritional value, and directly to landfills [43]. In the case of the seed, the extracts that it contains, such as starch, oil, antioxidants among others, represent a remarkable opportunity to generate added value products for potential applications, including textiles, biopolymers, bioenergy, cosmetic, brewery and so forth [43]. Ecuador is one of the many avocado producers and exporters in the continent. Despite being developed as a producer of the raw fruit, the avocado oil industry is not highly developed in the country. Uyama Farms is an ecuadorian company placed in Carchi, Imbabura, that specializes in avocado oil extraction, with its leading product named "MIRA", an extra virgin avocado oil. The company has an impact in the avocado production market and generates avocado seed waste daily [44]. Therefore, this biomass could be given an added value by being repurposed.

As previously mentioned, the Si/C ratio synthesis is 1:1, therefore an increased amount of carbon content represents a higher probability to obtain SiC. Monoliths synthesized by high internal phase emulsion can be obtained with different oily ohases (cyclohexane, n-hexane, dodecane and even recycled oil) [42, 45–52]

2.7.2 Recycled oil

Used cooking oil or waste cooking oil is a waste generated at large scales in industries and domestically. Its disposal is of immense importance, as it has the power to pollute bodies of water and soil. Therefore, ever since the 90's, research has been conducted to study the potential usage of used edible vegetable oil. Mainly, waste cooking oil has been used in soap production, the oleo-chemical industry and biofuels such as biodiesel and hydrogen gas [53, 54]. Waste cooking oil is composed of mostly triglycerides and its physicochemical properties depend on the process it undergoes when used for cooking; with longer usage resulting in higher acidity and viscosity [54]. In Ecuador, used cooking oil is usually collected by companies such as "PROGEDE OIL-NATURA", that recycle and transform

the waste material into raw material for biodiesel production [55]. Likewise, there are other authorized environmental manager companies that are responsible for the collection and recycling of this waste material. Private companies such as "La Fabril", further this task with various storage sites located in key provinces of Ecuador to collect the used oil for its exportation to European countries and further usage in biodiesel production [56]. Waste cooking oil has the potential to be used in other applications that also grant it an added value, therefore, the present work broadens the scope of the raw material as a carbon source for catalyst synthesis. To accomplish the goal of this project the following methodology was employed.

Chapter 3

Methodology

3.1 Materials and Reagents

The reagents employed on the synthesis of the silica monoliths and subsequent silicon carbide, were the following and were acquired from Sigma Aldrich: tetraethoxy-orthosilicate (TEOS) ($SiC_8H_{20}O_4$, purity 98%), Pluronic P123 (purity 99%), hydrochloric acid (HCl, purity 37%), zinc nitrate hexahydrate ($Zn(NO_3)_2 \cdot 6H_2O$, purity 98.5%), cobalt(II) nitrate hexahydrate ($Co(NO_3)_2 \cdot 6H_2O$, purity 98%), palladium(II) nitrate dihydrate ($Pd(NO_3)_2 \cdot 2H_2O$), sodium fluoride (NaF, purity 99%). The recycled palm oil was obtained from a nearby fast food restaurant; and the starch-less avocado seed was kindly donated by Uyamafarms S.A. and previously employed in the project "CEPRA XV-012-2021. Hacia la Economía Circular: Desarrollo de Eco-empaques a partir de residuos Agroindustriales", in which the seed's starch was removed for their aim.

The reagents employed for the reduction of 4-nitrophenol (4-NP) were the following: 4-nitrophenol ($C_6H_5NO_3$, purity 99%), hydrochloric acid (HCl, purity 37%), distilled water, sodium borohydride ($NaBH_4$, purity 98%)

For the kinetic studies on the adsorption of chromium(VI) were the following: potassium dichromate ($K_2Cr_2O_7$, purity 99.5%) and distilled water.

3.2 Synthesis of Silica Monoliths

The method employed for the synthesis of the silica monoliths functionalized with cobalt, zinc and palladium was based on the work of Vaca and Sommer [51] with some alterations,

employing avocado seed and recycled cooking oil as the carbon sources, metals as functionalizing agents and a PRO25D digital homogenizer to enhance the emulsion formation process. A 20% (w/w) P123 acidic solution of pH=2 was prepared and mixed with TEOS dropwise and stirred at 400 rpm at room temperature. The metallic nitrates and avocado seed were added simultaneously with the P123 in the aqueous phase for better dilution. This procedure originally takes 30 minutes, however, the current work required a period of about an hour and a half for the majority of the metal-functionalized silica monoliths. Once the hydrolysis of the silica precursor was finished, the solution was taken to a homogenizer and mixed with recycled palm oil (oil phase) dropwise after having NaF (8 gL^{-1}) added to improve the polymerization process and the pH regulation. The resulting content was deposited in 5 mL storage vials and kept at room temperature for a week for aging. See Figure 3.1 for an schematic representation of the aforementioned procedure.
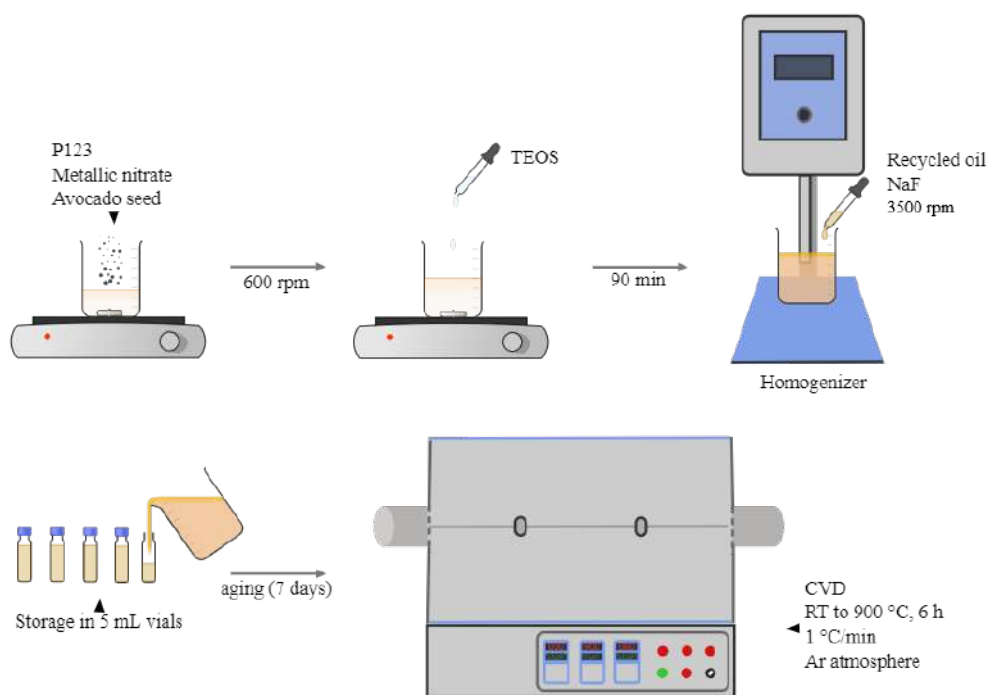

Figure 3.1: Schematic diagram of the experimental setup

3.3 Synthesis of Silicon Carbide

The aged monoliths were pyrolyzed in the Chemical Vapor Deposition (CVD) equipment, which is a MTI Co. OTF-1200X tube furnace with a quartz tube, with a temperature ramp

from room temperature up to 900 °C and heating rate of 1 °C/min for a period of 6 hours in an argon atmosphere. The resulting calcined monoliths were restored into its original vial containers and kept at room temperature. This procedure not only produces silicon carbide from the silica precursor (TEOS) and the carbon precursor (avocado seed and recycled oil) but also frees the mesoporosity of the monoliths by eliminating the remaining P123. A variety of samples were synthesized and functionalized with different metals, oil phases and quantity of avocado seed; Table 3.1 compiles the most revelant of the synthesized monoliths.

Table 3.1: Nomenclature for the synthesized SiC monoliths and their main characteristics

Code	Oil phase	Seed quantity (mg)	M (II)
cSiC	cyclohexane	-	-
cSiCZC	cyclohexane	-	Zn, Co
cSiC50	cyclohexane	50	-
oSiC	recycled oil	-	-
oSiC50	recycled oil	50	-
oSiC50ZC	recycled oil	50	Zn, Co
oSiC50P	recycled oil	50	Pd
oSiC100	recycled oil	100	-
oSiC100ZC	recycled oil	100	Zn, Co
oSiC100P	recycled oil	100	Pd

3.4 Characterization Techniques

The techniques used for this work were: X-ray Photoelectron Spectroscopy (XPS), Attenuated Total Reflection Fourier Transform Infrared Spectroscopy (ATR-FTIR), X-ray Fluorescence (XRF), X-ray Powder Diffraction (XRD), UV-Vis Spectroscopy (UV-Vis) and Atomic Absorption Spectroscopy (AAS).

3.4.1 UV-Vis Spectroscopy (UV-Vis)

UV-Vis Spectroscopy is a technique for the analysis of solids and powders to obtain molecular spectroscopic information. It is used in the ultraviolet, visible and infrared regions of the light spectrum and requires limited sample preparation [57]. This technique outcasts the absorption or reflectance spectra of a sample when exposed to light in a determined

range of the electromagnetic spectrum [58]. In order to perform this characterization technique, the PerkinElmer LAMBDA 1050+ UV/Vis/NIR Spectrophotometer was used with the liquid samples module in the range of 250 cm^{-1} to 500 cm^{-1}.

3.4.2 Attenuated Total Reflection Fourier Transform Infrared Spectroscopy (ATR-FTIR)

Infrared Spectroscopy (IR) is a technique highly employed for the determination of molecular composition and structure. The ATR-FTIR technique helps provide this information with a higher sensitivity to the surrounding fluctuations without the need for extensive sample preparation as in the case of conventional FTIR spectroscopy [59]. The technique was used employing the Agilent Cary 630 FTIR Spectrometer with Attenuated Total Reflectance (ATR) as the sampling module with diamond tip, and in the infrared region between 650-4000 cm^{-1}.

3.4.3 X-ray Powder Diffraction (XRD)

XRD spectroscopy is a technique that allows the examination of the chemical composition and structure of solids by means of radiating an x-ray beam onto the surface of a sample to obtain quantitative information about the crystallinity of the material [60]. The XRD characterization was carried out employing the MiniFlex600 X-ray diffractometer from Rigaku with D/tex Ultra2 detector. The diffraction patterns were obtained in the 2θ range of 15°- 60°with a step of 0.005. It is important to consider that, for this technique only the calcined samples were tested.

3.4.4 X-ray Photoelectron Spectroscopy (XPS)

XPS spectroscopy is a technique for surface analysis by irradiating the surface of a solid with x-rays and analyzing the released electrons by energy. This is handy in the identification of elements, analysis of chemical composition and identification of chemical state [61]. The equipment employed for the characterization technique was a PHI Versa-Probe III 5000 photoelectron spectrometer under high power mode. The spectra was obtained using Al Kα X-rays with a photon source energy of 148.66 eV and high vacuum conditions.

The SiC monolith samples were evaluated for two main applications: Cr(VI) adsorption and hydrogen production, so as to corroborate its main properties, previously described in Section 2.3.

3.4.5   X-ray Fluorescence analysis (XRF)

X-ray fluorescence spectrometry is a non-destructive technique that determines the chemical composition of compounds. It is highly accurate and usually used in elemental composition analysis in fields such as geology and materials [62]. This analysis was performed in the Otavalo installations of UNACEM, a well-established cement factory that kindly lend their equipment for the study. The device employed was a high Performance Wavelength dispersive S8 TIGER Series 2 WDXRF XRF spectrometer.

3.4.6   Atomic Absorption Spectroscopy (AAS)

The AAS is a technique that qualitatively and quantitatively determines the presence of elements in a sample, by applying the absorption of radiation by free atoms in a gaseous state [63]. The AAS characterization was carried out employing the Analytik Jena contrAA 700 Atomic Absorption Spectrometer, model 161K0915.

3.5   Chromium (VI) adsorption evaluation

A set of sorption experiments were conducted to examine the effect of time of contact as a variable. In broad terms, the experiments consisted on the adsorption of Cr(VI) from a 10 ppm potassium dichromate solution by silicon carbide ($\sim$20 mg) during a determined set of time intervals. With the help of an atomic absorption spectrometer, a calibration curve was first constructed as a means to relate the absorbance of the treated solution to its concentration, thus performing a quantitative analysis of the adsorption reaction. Refer to Figure 3.2 to observe a block diagram with the main details of the procedure.

Then for the adsorption kinetics were performed analogous to the work of [64], the amount of chromium (VI) adsorbed per gram of adsorbent through time (q) was calculated with Equation 3.1.
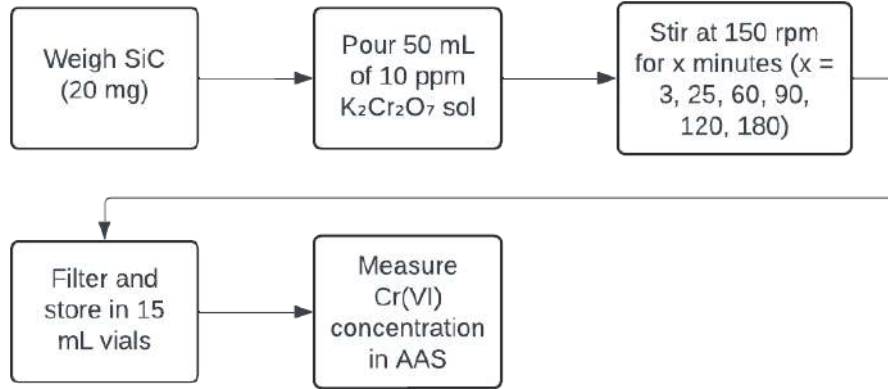
Figure 3.2: Block diagram of the experimental procedure for adsorption evaluation

$$q = \frac{(C_0 - C_t)V}{m} \tag{3.1}$$

Where C_0 and C_t refer to the initial and final concentrations (mgL^{-1}) of the chroumium (VI) solution; V (L) refers to the volume of the solution and m to the mass (mg) of the adsorbent employed.

Subsequently, the data obtained was fitted to two kinetic models, pseudo-firs-order (PFO) and pseudo-second-order (PSO), which would determine if the adsorbate and adsorbent interact through chemisorption or physisorption. The linearized equation for PFO is shown in Equartion 3.2, and the linearized equation for PSO, in Equation 3.3 [65, 66].

$$\ln(q_i - q_{i-1}) = \ln(q) - k_1 t \tag{3.2}$$

$$\frac{1}{q} = \frac{1}{k_2 q^2} \cdot \frac{1}{t} + \frac{1}{q} \tag{3.3}$$

Where k_1 and k_2 refer to the equilibrium rate constant $(Lmin^{-1})$ of the PFO and PSO model, respectively.

3.6 Photoconversion of 4-nitrophenol (4-NP)
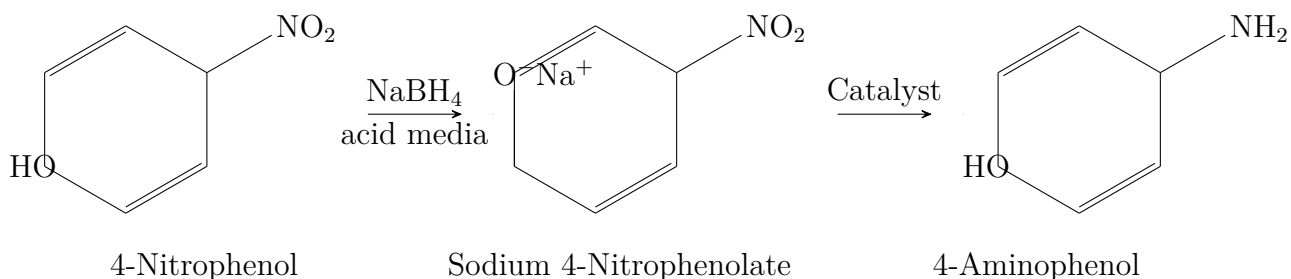
Scheme 1: Reduction of 4-nitrophenol to 4-aminophenol.

The catalyst-assisted photoconversion of 4-nitrophenol in the presence of sodium borohydride (Scheme 1) was performed to analyze the reduction capacity of SiC as a catalyst. The catalyst's aid in the reduction reaction implies that it acts as an intermediate in the transfer of hydrogen from sodium borohydride to 4-NP. This alludes to the existence of active sites in the catalyst that can adsorb and activate hydrogen species. Consequently, such a catalyst is potentially effective in reactions that entail the production of hydrogen [67, 68]. Therefore, the photocatalytic capacity of silicon carbide was studied for the aforementioned reaction.

The reaction was performed following the procedure of Hernández-Gordillo [69], with certain variations. The photocatalytic conversion reaction was carried out in a 250 mL borosilicate glass bottle containing 200 mL of a 7.5 ppm 4-NP acidic solution, 0.5 M of $NaBH_4$ and 0.075 gL^{-1} of photocatalyst (SiC). The mixture was agitated with a magnetic stirrer (600 rpm) for 30 minutes at room temperature and in the absence of light (covered by tin foil). Subsequently, the container was irradiated with UV light in a UV-lamp chamber with a high-pressure Hg lamp emitting 356 nm of 4400 $\mu W cm^{-2}$, without the tin foil cover and with no cap for better exposure. A series of 3 mL samples were extracted from the solution in intervals of 10 minutes until reaching 60 minutes. Afterwards, the concentration of the samples were estimated through UV-Vis spectroscopy in the range of 250-500 nm to follow the disappearance of the absorption band at around 400 nm or the appearance of the absorption band at around 290 nm, which would indicate the reduction of 4-NP.

Chapter 4

Results and Discussion

The raw materials employed for the synthesis of the silicon carbide, namely starch-less avocado seed and recycled palm oil, were greatly leveraged in the synthesis process of the material and given the characterization techniques and the applications for which the SiC samples were evaluated, the following results were obtained.

4.1 Characterization of raw materials

4.1.1 Avocado seed

In Figure 4.1, the appearance of the starch-less avocado seed is portrayed. As previously mentioned, the seed was obtained from a previous research project after its utilization in the production of starch-based polymers.

Figure 4.1: Physical aspect of avocado seed (raw material).

Figure 4.2 showcases the spectra of starch-less avocado seed. The band at 3300 cm^{-1} represents the O-H group from the hydrogen bonds of alcohols in lignin and cellulose; at 2924 cm^{-1} is attributed to C-H stretching; the peaks at 1614 cm^{-1} and 1516 cm^{-1} are the stretching vibrations of the C=O group and the structural vibrations of the C=C bonds of lignin [70]. The peak at 1438 cm^{-1} is assigned to aliphatic bending vibrations, while the peaks in the range of 1374 cm^{-1} to 1015 cm^{-1} correspond to the C–O stretching vibrations of alcohols, phenols, ethers and esters groups [70].
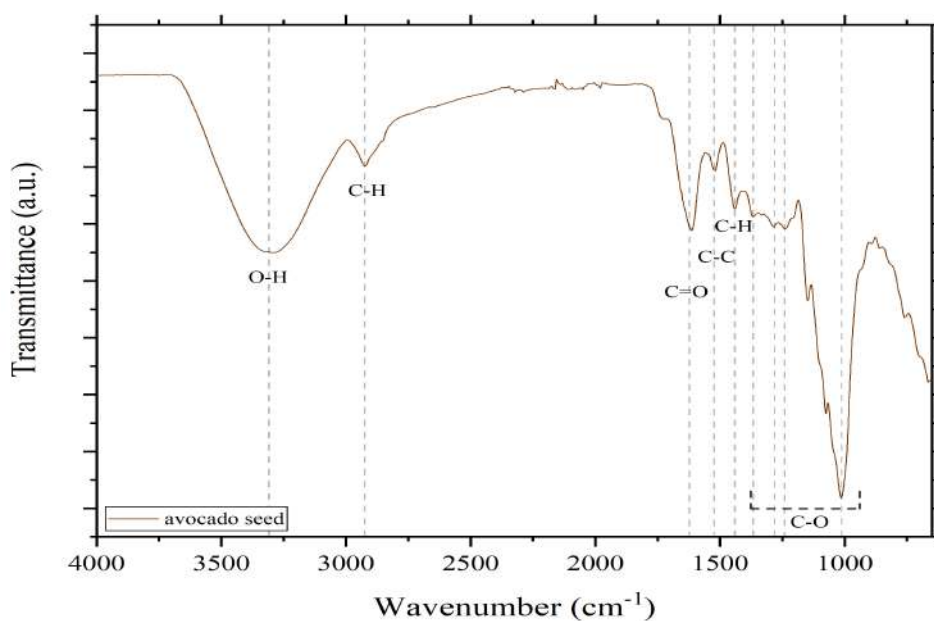
Figure 4.2: ATR-FTIR spectrum of avocado seed.

Due to the powder form of the avocado seed, an XRD diffractogram was also obtained as a mean of further characterization. Figure 4.3 presents the aforementioned diffratogram. There is a broad peak at around 22°that denotes a major amorphous phase of the compound, mainly it is related to polysaccharides found in avocado seed, such as cellulose, hemicellulose, lignin among other non-starch polysaccharides; on the contrary, there are two peaks of sharper nature, which could be ascribed to crystalline cellulose regions [71–73].

Figure 4.3: XRD diffractogram of starch-less avocado seed.

4.1.2 Recycled cooking oil

In Figure 4.4, an image of recycled palm oil employed can be appreaciated. The material was kindly supplied by a local restaurant and filtered of solids.

Figure 4.4: Physical aspect of recycled palm oil (raw material).
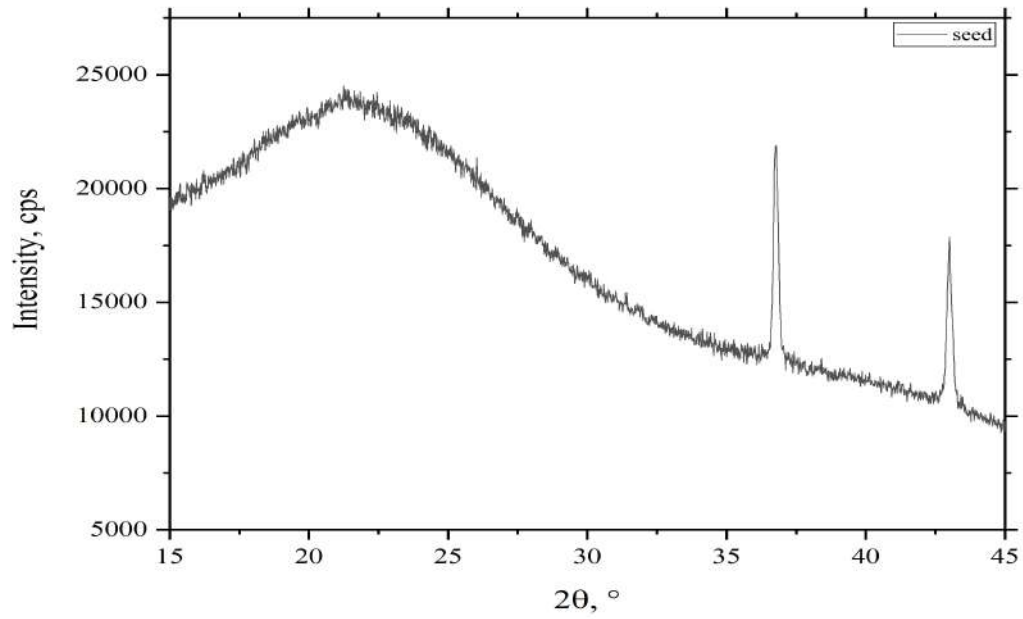
Recycled palm oil's FTIR spectrum has been previously reported [74]. Figure 4.5 represents the ATR-FTIR spectra of the recycled oil employed in the synthesis process. The organic molecule exhibits C-H symmetrical and asymmetrical stretching vibrations in the 3009-2845 cm^{-1} region. From 1464 cm^{-1} to 1380 cm^{-1}, there are peaks corresponding to bending vibration of the alkane group (C-H). In the lower region of the spectrum, there is a peak that is ascribed to the rocking vibration of CH_2 groups. In the 1464-1380 cm^{-1} region, the presence of C-H group is observed through the elucidation of scissoring vibration in CH_2 groups, bending vibrations in CH_3 groups and symmetric bending of CH_3 groups [75].

Additionally, the ester groups present in triglycerides appear at 1745 cm^{-1}, 1236 cm^{-1}, 1165 cm^{-1}, 1119 cm^{-1} and 1093 cm^{-1}; peaks that are assigned to stretching vibrations of C=O groups, C-O stretching or C-C stretching, belonging to the fatty acid chains, and asymmetric C-O stretching vibrations [75].
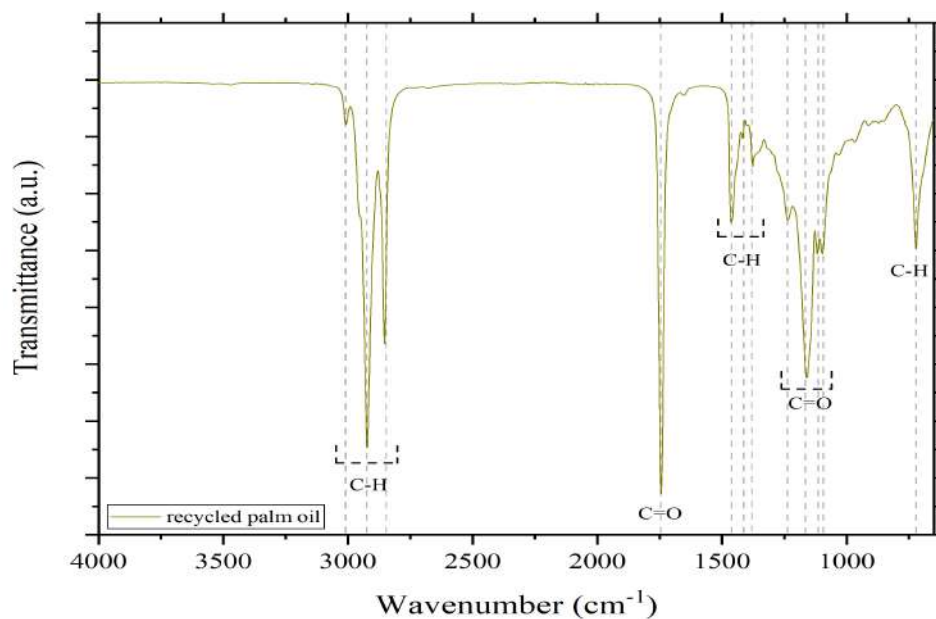

Figure 4.5: ATR-FTIR spectrum of recycled palm oil.

Once the main properties and characteristics of the raw materials were studied, a comparison between agitation method, oil-phase and seed quantity was carried out.

4.2   Synthesis Analysis

4.2.1   Silica Monoliths (SiO_2)

The first silica monoliths synthesized with cyclohexane as the oil phase were mostly white with a chalk-like appearance. Figure 4.6 exhibits cSiC monoliths made with (upper left) and without (upper right) the help of a homogenizer for the mixing of the oil phase, as well as a cSiC50 monolith. All of which display the characteristics mentioned as well as fine cracks that generated during the drying and aging process due to the evaporation of the cyclohexane. Particularly, the monolith shown in the upper right, obtained with a magnetic stirrer in a hot plate, has a wrinkled aspect, which could be attributed to an early evaporation of the oil phase from the solution during the mixing process, due to the more extended time the process took in the homogenizer. It was noticed that the amount of seed could not be increased to 100 mg per monolith with cyclohexane as the oil phase owing to its early evaporation and to the great water absorption capacity of avocado seeds (more than twice its weight) which turned out in the completely absorption of the water phase, thus hindering the emulsion performance. From then on, all monoliths were synthesized employing recycled cooking oil as the oil phase because it was generating an oily layer around the avocado seed preventing aqueous phase to be absorbed.

Figure 4.6: Image of cSiC (above) and cSiC50 (below) monoliths

The synthesized oil-based silica monoliths displayed an orange-ish color due to prevalence of the intrinsic color of the oxidized avocado seed, with the exception of the silica

monoliths functionalized with palladium, which gray color prevailed over the orange. Over-all, these monoliths are sturdier than the ones synthesised before.The physical character-istics mentioned can be better appreciated in Figure 4.7. The texture of the mixture of the monoliths previous to aging was thicker when increasing the amount of avocado seed and in comparison with the cyclohexane-based silica monoliths. Therefore, recycled palm oil was employed as the oil phase for the SiC synthesis.

Figure 4.7: Image of oSiC (left) and oSiCZC (right) before calcination.

4.2.2 Silicon Carbide (SiC)

Considering that all pyrolyzed monoliths are oil-based, which results in a higher carbon content, the resulting oSiC monoliths depicted a shiny outside with an opaque inside and a moderate brittleness; this was congruous among all the samples and compositions. Figure 4.8 presents the images of oSiC and oSiC50 monoliths, from with small differences between them can be pinpointed. Primarily, there is a more lustrous look to the oSiC50 monolith, likely due to the higher content of carbon thanks to the addition of avocado seed.

Figure 4.9 depicts oSiC50 and oSiC100 monoliths, at first sight these share the same aspect, therefore, their differences are further studied with different characterization tech-niques.

Figure 4.8: Image of oSiC (above) and oSiC50 (below) monoliths

Figure 4.9: Image of oSiC50 (above) and oSiC100 (below) monoliths

4.3 Characterization of SiC monoliths

4.3.1 Composition

X-ray photoelectron spectroscopy (XPS)

The surface elemental composition was analyzed via XPS. All the samples analyzed from the pyrolyzed monoliths and displayed the presence of three main elements: C1s, O1s and Si2p, which are expected of both SiO_2 and SiC [76]. The characteristics peaks of O1s

appear at 978.11 eV and 529.95 eV, for C1s a less prominent peak appears at around 282.62 eV and two small-intensity peaks at 151.84 eV and 102.87 eV elucidate the presence of Si2p [61]. It is pertinent to mention that due to the reaching extent of the technique (50-70 Å) and the low concentration of the metals in the material (0.01 M/Si molar ratio; M=Zn/Co, Pd), the metal oxides were not observable. Further characterization was performed to confirm the presence of the metallic species in the compound.

Figure 4.10 highlights the full-range spectra of oSiC50, oSiCZC50 and oSiCP50 monoliths. The oSiC50 monolith presents C1s, O1s and Si2p percentage composition of 6.9%, 68.1% and 25% respectively. The oSiCZC50 a composition of 49%, 38.9% and 12.1%; and oSiCP50 a content of 39%, 45.2% and 15.8% respectively. The significant O 1s content difference between oSiC and oSiCM (M=Zn/Co, Pd) could be attributed to the formation of metal oxides, which would lead to the decrease of the amount of detectable O 1s in the surface of the material.

Figure 4.11 showcases the elemental composition of oSiC100, oSiCZC100 and oSiCP100 monoliths. A different behaviour is observed in this case, as the monolith with lesser amount of O 1s is oSiCZC100 with a percentage composition of 37.8%, 45.5% and 16.7% for C1s, O1s and Si2p respectively. For oSiC100 and oSiCP100 the percentages are 41.5%, 42.1%, 16.4% and 43.9%, 41.2%, 14.9% respectively.

A deconvolution analysis was performed for each constituent. Regarding the spectrum of C1s, four peaks are proposed at around 282.6 eV, 284.8 eV, 286 eV and 288 eV respectively. These are ascribed to Si-C, C-C, C-O and C=O groups, with all carbon-containing groups being attributed to adventitious carbon contamination [77–79]. Table 4.1 illustrates the B.E.s values at which the characteristic C1s groups are found in the spectrum, as well as the percentage of area of each peak. Comparing the monoliths containing 50 mg and 100 mg of avocado seed, the content of carbon rises with avocado seed content, as expected. The deconvolution and area of the peaks can be better appreciated in Figure 4.12 and Figure 4.13.

The spectrum of O1s, shown in Figure 4.12 and Figure 4.13, proposes two peaks at around 530 eV and 533 eV that correspond to M_xO_y (M=Zn/Co, Pd) due to metal-oxygen interactions and Si-O groups, respectively [79, 80]. Likewise, the spectrum for Si2p shows two peaks at around 100 eV and 103 eV that can be associated with Si-C and Si-O groups

Table 4.1: XPS B.E.s, chemical group and area percentage of all SiC samples

| Sample		oSiC50			oSiC100	
Element	Group	B.E. (eV)	Area (%)	Group	B.E. (eV)	Area (%)
C1s	Si-C	282.60	22.09	Si-C	282.80	35.82
	C-C	284.80	55.47	C-C	284.20	55.07
	C-O	286.20	9.42	C-O	286.00	4.97
	C=O	287.70	13.02	C=O	288.00	4.15
O1s	MxOy	530.40	17.86	MxOy	530.40	22.11
	Si-O	533.50	82.14	Si-O	531.90	77.89
Si2p	Si-C	100.70	17.23	Si-C	101.30	34.45
	Si-O	104.10	82.77	Si-O	102.70	65.55
Sample		oSiCZC50			oSiCZC100	
C1s	Si-C	282.60	51.74	Si-C	282.80	65.21
	C-C	284.30	37.31	C-C	284.30	28.08
	C-O	286.00	5.45	C-O	286.00	1.82
	C=O	288.00	5.51	C=O	288.00	4.89
O1s	MxOy	530.29	38.75	MxOy	529.80	22.87
	Si-O	532.01	61.25	Si-O	531.30	77.13
Si2p	Si-C	100.70	24.42	Si-C	100.90	43.39
	Si-O	102.20	75.58	Si-O	102.20	56.61
Sample		oSiCP50			oSiCP100	
C1s	Si-C	283.00	45.19	Si-C	282.90	77.94
	C-C	284.80	35.63	C-C	284.50	10.30
	C-O	286.00	11.61	C-O	285.90	6.63
	C=O	288.00	7.57	C=O	288.00	5.14
O1s	MxOy	531.40	57.83	MxOy	530.40	25.52
	Si-O	533.00	42.17	Si-O	531.40	74.48
Si2p	Si-C	100.70	50.92	Si-C	101.00	23.66
	Si-O	102.30	49.08	Si-O	102.00	76.34
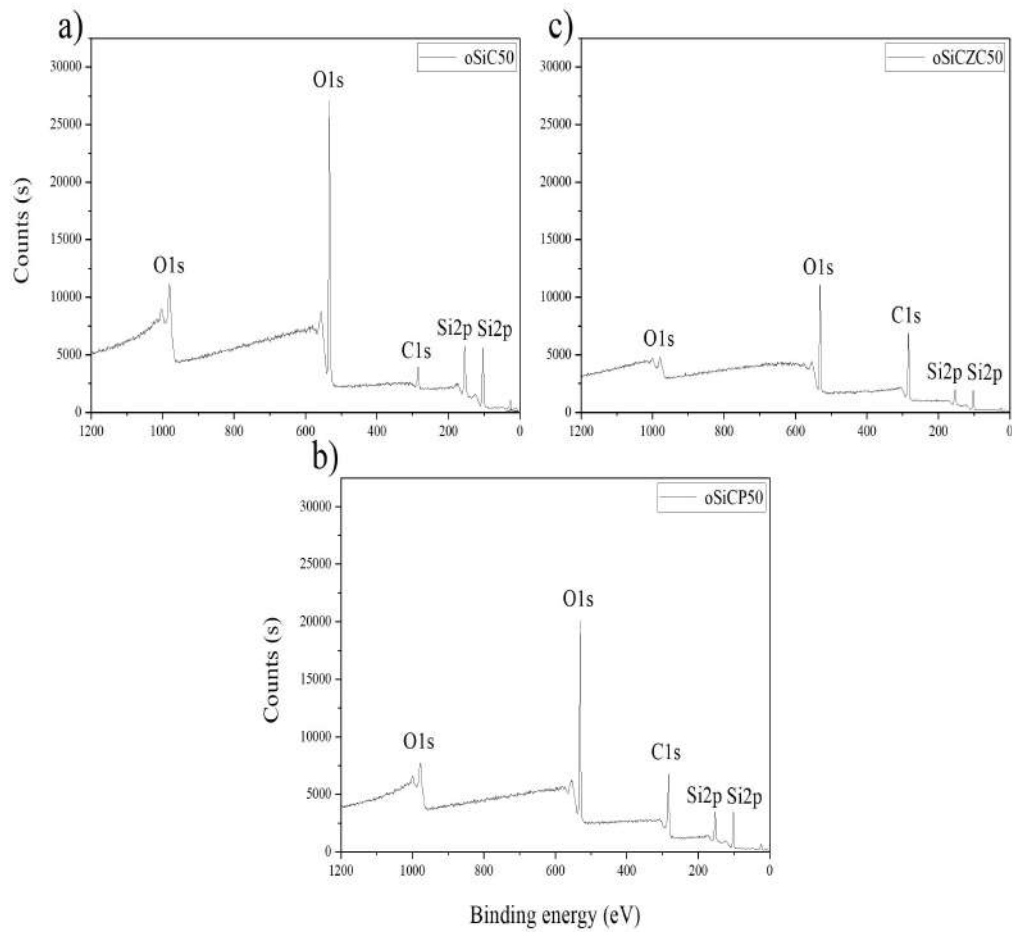
Figure 4.10: XPS spectra of a) oSiC50, b) oSiCP50 and c) oSiCZC50.

[79, 81].

Figure 4.12 illustrates the content of each group per constituent for the monoliths with 50 mg of avocado seed. In particular, the content of adventitious carbon found in the SiC material is greater for the oSiC50 monolith, which could be credited to a higher level of contamination due to a longer exposure to the environment coupled with a lower content of crystalline SiC. The content of Si-O in both O1s and Si2p constituents is at its maximum for the same sample, which would be in accordance with the low levels of Si-C.
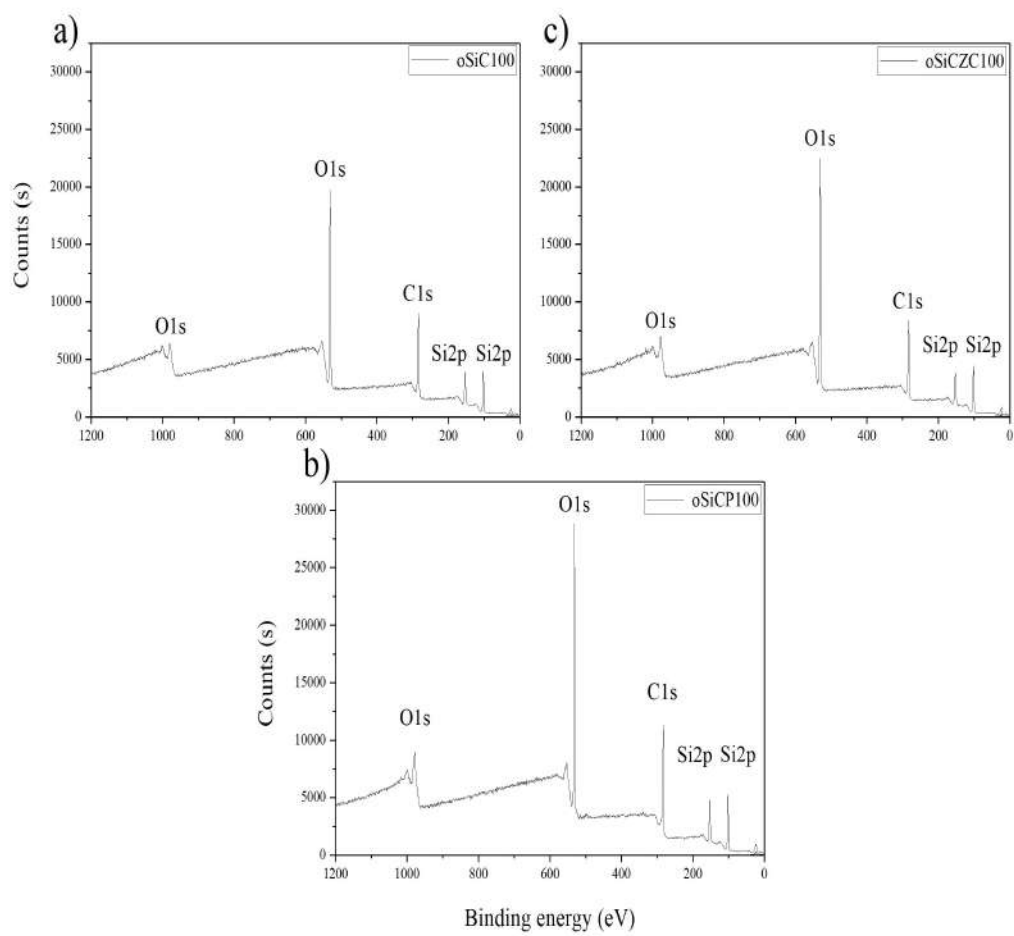
Figure 4.11: XPS spectra of a) oSiC100, b) oSiCP100 and c) oSiCZC100.
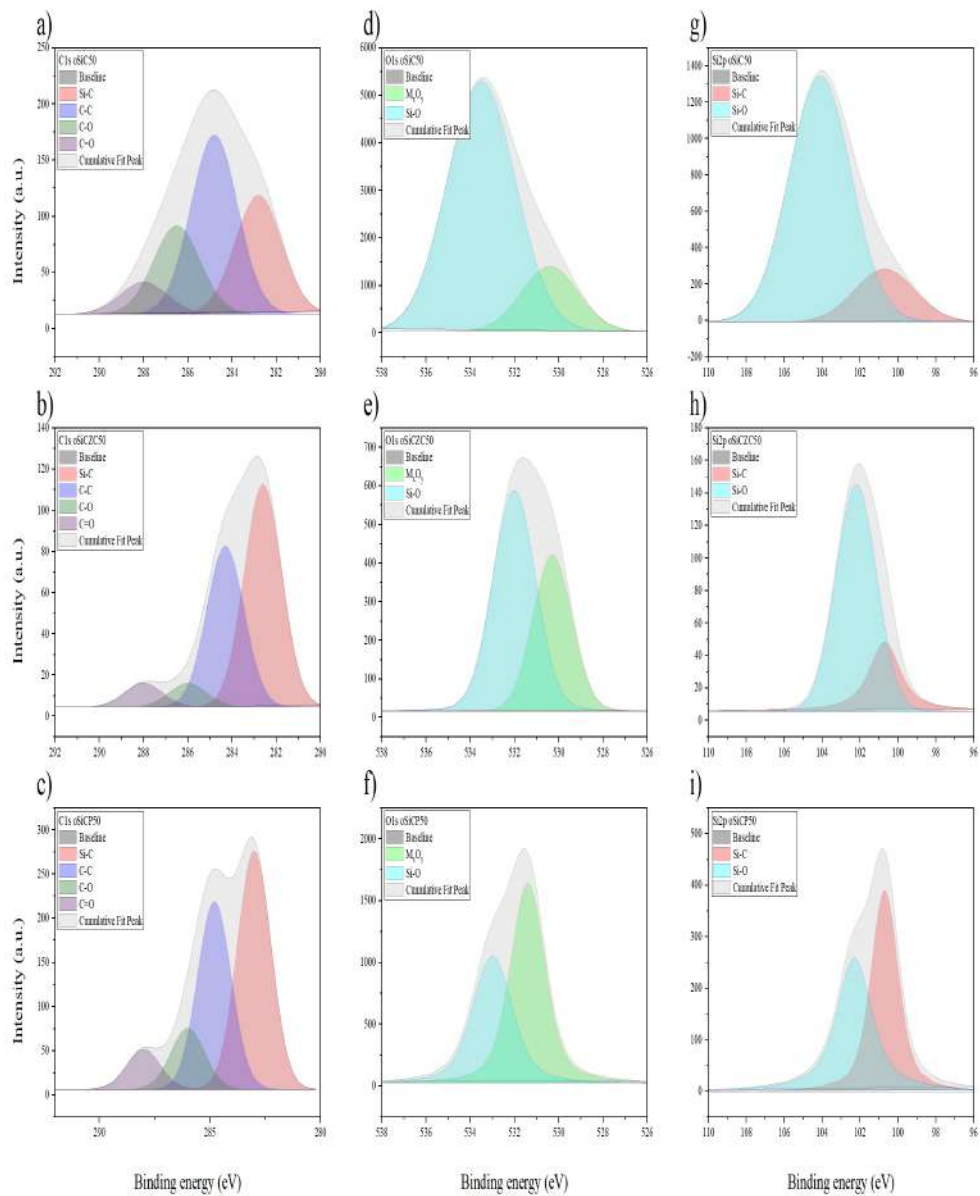
Figure 4.12: XPS deconvolution spectra of a) C1s oSiC50, b) C1s oSiCZC50, c) C1s oSiCP50, d) O1s oSiC50, e) O1s oSiCZC50, f) O1s oSiCP50, g) Si2p oSiC50, h) Si2p oSiCZC50, i) Si2p oSiCP50.
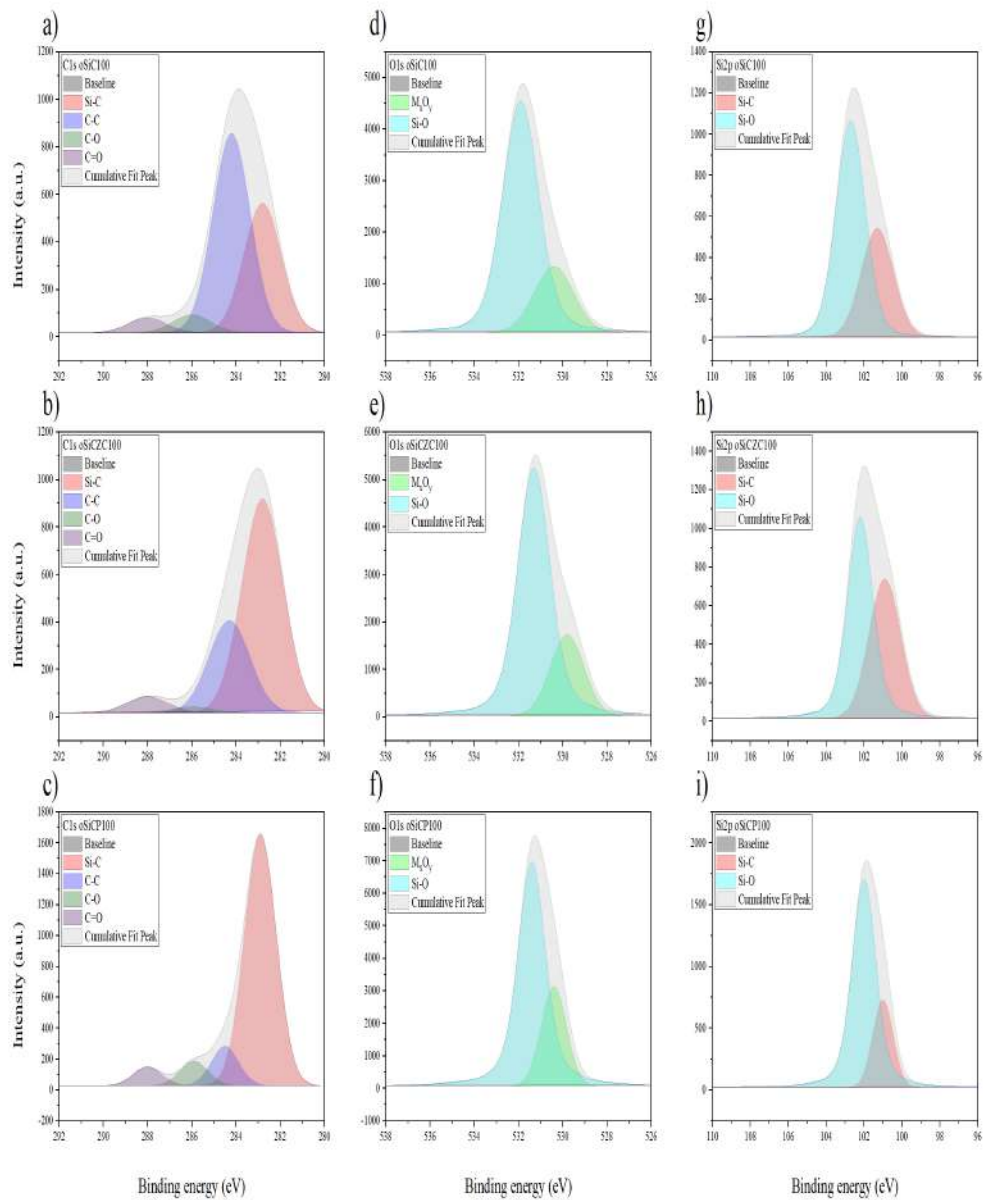
Figure 4.13: XPS deconvolution spectra of a) C1s oSiC100, b) C1s oSiCZC100, c) C1s oSiCP100, d) O1s oSiC100, e) O1s oSiCZC100, f) O1s oSiCP100, g) Si2p oSiC100, h) Si2p oSiCZC100, i) Si2p oSiCP100.

As expected, Figure 4.13 and Table 4.1 highlight larger area Si-C peaks for the monoliths composed of 100 mg of avocado seed. Therefore, at larger amount of carbon in the composition, there is a more significant conversion of SiO_2 to SiC.

Attenuated Total Reflection Fourier Transform Infrared Spectroscopy (ATR-FTIR)

The silica monoliths were studied through ATR-FTIR before and after calcination; Figure 4.14 showcases the spectra obtained for the samples synthesized with 50 mg of avocado seed before and after pyrolyzation. Before calcination, at 3300-3028 cm^{-1} there is a broad band that corresponds to the stretching vibration of the O-H group. The group that is characteristic of water it is also seen at around 1639 cm^{-1} and 1337 cm^{-1} but is attributed to water of crystallization that is embedded in the compound's structure. In the region of 2922 cm^{-1} to 2850 cm^{-1}, the doublet can be attributed to the symmetric and asymmetric stretching of C-H in methylene (CH_2) groups. Particularly, the symmetric stretching vibrations can be attributed either to the surfactant (P123) or the recycled palm oil, both organic molecules. The peak at 1736 cm^{-1} can be ascribed to the stretching of ester group (C=O) and the peak at 1143 cm^{-1}, to C-O stretching. At 1456 cm^{-1}, 1371 cm^{-1} and 719 cm^{-1}, the observed peaks correspond to the scissoring vibration of the C-H bonds in methylene groups, symmetric bending of CH_3 groups and rocking vibrations of methylene groups, respectively. The region from 1071 cm^{-1} to 797 cm^{-1} comprises the presence of Si bonds, particularly Si-O-Si stretching and Si-OH groups [75].

After the calcination process, a low intensity, moderately-sharp peak can be observed at around 803 cm^{-1}; the band could correspond either to Si-C or Si-O-Si stretching vibrations. On account of the previous results from the XPS analysis, the presence of Si-C could be suggested and is also in accordance with the wavenumber values reported for bulk SiC [82]. It can also be inferred that there is still a high prevalence of silica (SiO_2) in the pyrolyzed monoliths due to the high intensity of the peak at around 1065 cm^{-1}, which may refer to the Si-O-Si bond of the amorphous silica that remained unchanged after the thermal treatment. Contrarily, the Si-OH groups disappeared after the thermal treatment, which further supports the presence of Si-C groups [75].

Figure 4.14: ATR-FTIR spectra of oSiC50, oSiCZC50 and oSiCP50 a) before calcination and b) after calcination.

Figure 4.15 displays the same characterization for the monoliths containing 100 mg of avocado seed. The monoliths before calcination show the same characteristic peaks of organic molecules (P123, oil and avocado seed). Analogously, the presence of Si-O-Si and Si-C is prevalent in the pyrolyzed monoliths. Additionally, a weak peak can be discerned at around 2097 cm^{-1} and 1575 cm^{-1}, which are proposed to correspond to C-H and C=C stretching vibrations. These are common unreacted carbonaceous materials [75].
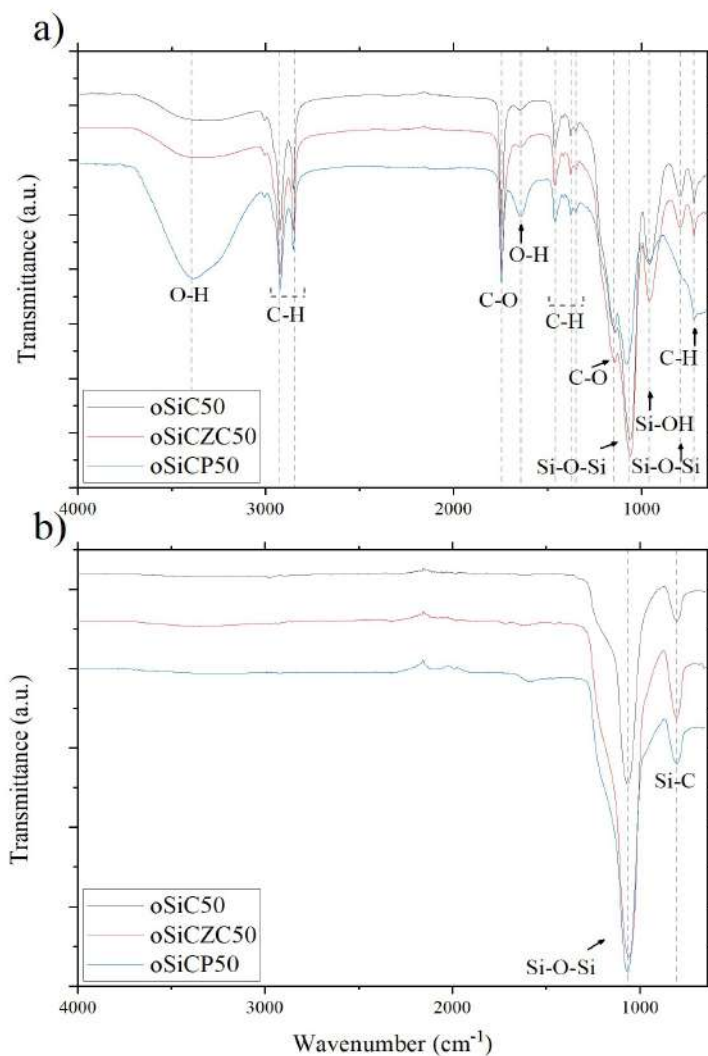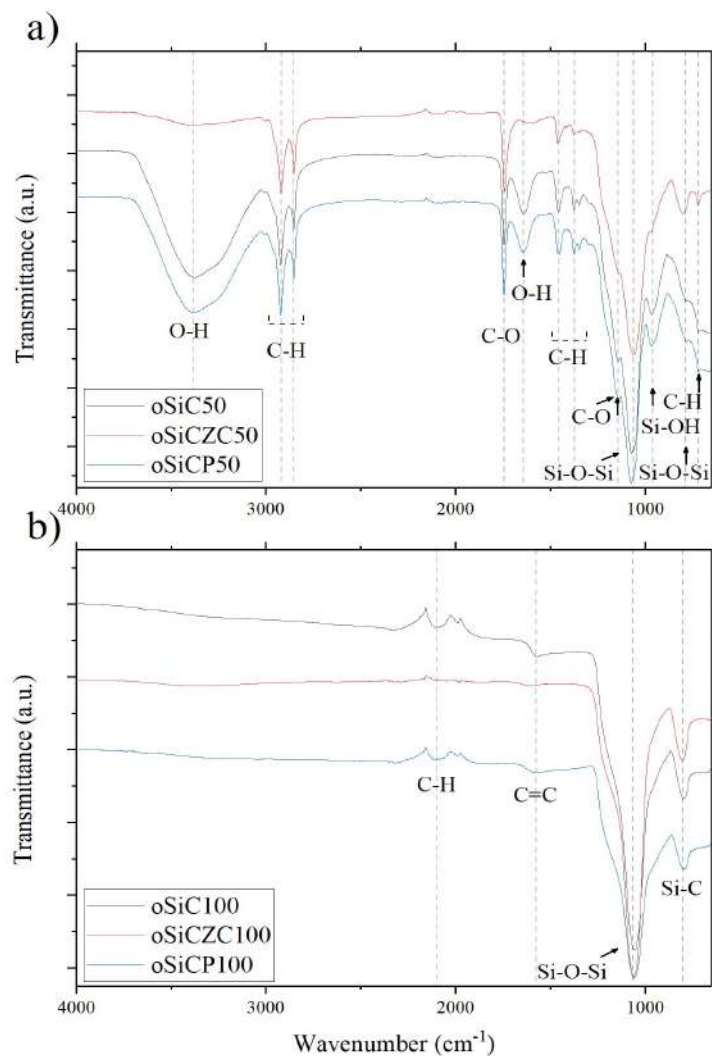
Figure 4.15: ATR-FTIR spectra of oSiC100, oSiCZC100 and oSiCP100 a) before calcination and b) after calcination.

From the ATR-FTIR characterization method, no further conclusions could be drawn. However, it can be denoted that there is a difference in the intensity of the Si-C peak, which is heightened with a higher amount of carbon, which favours the generation of SiC.

X-ray Fluorescence (XRF)

The XRF analysis shown in Table 4.2 exhibited the high silicon content of the majority of the samples and confirmed the presence of metals. The oSiCP100 monolith had the highest

percentage of palladium (II) and oSiCZ100 the highest content of cobalt (II), although a small amount for the overall composition. The rest of the elements appearing in the analysis are a result of the several treatment procedures that the avocado seed underwent in the previous project it was employed in. Additionally, contamination was most likely to happen in the industry plant due to the raw material used. It is worth noting that an analysis to look for organic compounds was conducted on one of the monoliths, oSiC50, and revealed a high carbon content (see Table 6.1 in Chapter 6).

Table 4.2: XRF elemental analysis

Element	Concentration (%)					
	oSiC50	oSiCP50	oSiCZC50	oSiC100	oSiCZC100	oSiCP100
Si	95.47	92.41	67.75	91.71	12.23	45.47
Al	0.09	0.13	0.47	0.60	0.01	0.22
Fe	0.74	1.21	5.22	2.20	0.66	1.83
Ca	2.04	2.69	14.60	3.55	0.13	3.93
P	1.22	2.60	0.45	0.40	0.04	0.30
K	0.16	0.27	0.89	0.77	0.15	1.07
Cr	0.10	0.15	0.55	0.38	0.08	0.25
S	0.07	0.12	0.40	0.15	0.01	0.17
Ti	0.04	-	-	-	-	-
Mn	0.03	0.04	0.14	-	0.01	-
Mo	0.02	-	-	-	-	-
Cu	0.02	0.02	-	0.05	-	0.55
Zn	0.01	0.04	0.10	0.03	-	3.38
Na	-	0.04	0.10	0.12	-	-
Co	-	0.30	-	-	0.48	-
Pd	-	8.97	-	-	-	42.26
Ni	-	-	0.07	-	-	-
V	-	-	0.10	-	-	-
Mg	-	-	0.19	-	-	-
Ru	-	-	-	0.05	-	-
Rh	-	-	-	-	-	0.50
As	-	-	-	-	-	0.07

4.3.2 Structure of SiC

X-ray Powder Diffraction (XRD)

The XRD spectra for oSiC50 monoliths shown in Figure 4.16 exhibits, primarily, a broad peak that is distinctive to the amorphous phase of silicon oxide [83]. In oSiCP50, there is a clear peak at around 24.14°, which could correspond to unreacted Si [84]. With respect to the presence of crystalline silicon carbide, there are two main peaks at 32.26° and 35.31°, that could be attributed to β-SiC [84], observable with high intensity values for oSiCP50 and almost imperceptible low intensity peaks for oSiC50 and oSiCZC50. For the oSiCP50 monolith there are also strong peaks that could be ascribed to palladium (II) oxide [85].
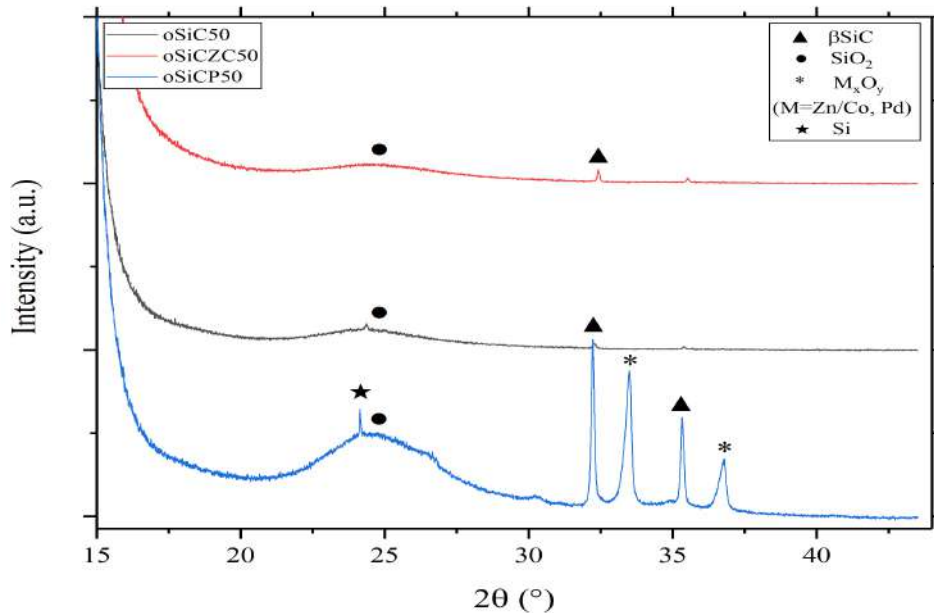

Figure 4.16: XRD spectra of oSiC50, oSiCZC50 and oSiCP50.

In the case of oSi100 monoliths, which spectra is shown in Figure 4.17, there is a perceptible increase in the intensity of the peaks shown in all samples. Despite the higher carbon content, the amorphous phase is still present in the form of the broad band at 2θ values around 22°. A strong peak is shown at around 37.5° for oSiC100 and oSiCP100, which could be assigned to β-SiC [84]. Similarly, a peak at around 43.71° shows great intensity and sharpness and could also be attributed to the characteristic peaks of β-SiC [84]. Both peaks are shifted in the spectrum of the oSiCZC100 monolith. Additionally,

in the particular case of oSiCP100 shows a moderately sharp peak at around 41.73° which could signify the prevalence of palladium (II) oxide in the material [85].
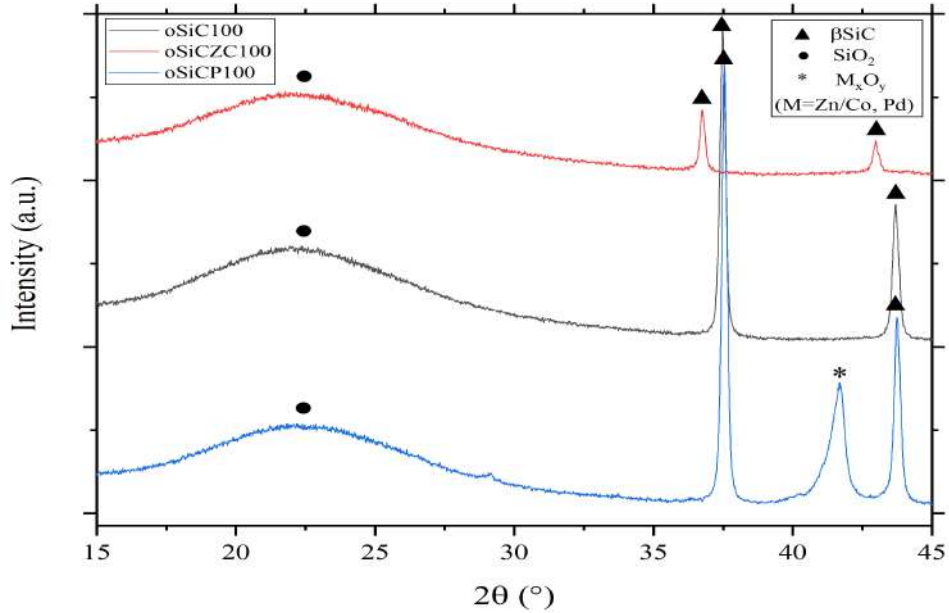

Figure 4.17: XRD spectra of oSiC100, oSiCZC100 and oSiCP100.

Following the characterization techniques to determine the composition and structure of the silicon carbide monoliths, the application evaluation results are present in the following sections.

4.3.3 Applications of SiC

Chromium (VI) adsorption evaluation

Figure 4.18 shows the chromium (VI) adsorbed by the monolith through time. Most samples show similar results, at low adsorption levels; however, oSiCZC100 monolith was the one that had the greatest adsorption capacity among all the monoliths and had a high accuracy between samples from the same batch. The kinetic behavior of the data for all monoliths is mostly not consistent through time thus, the fitting to the PFO and PSO kinetic models is presented in Figure 4.19 and Figure 4.20.
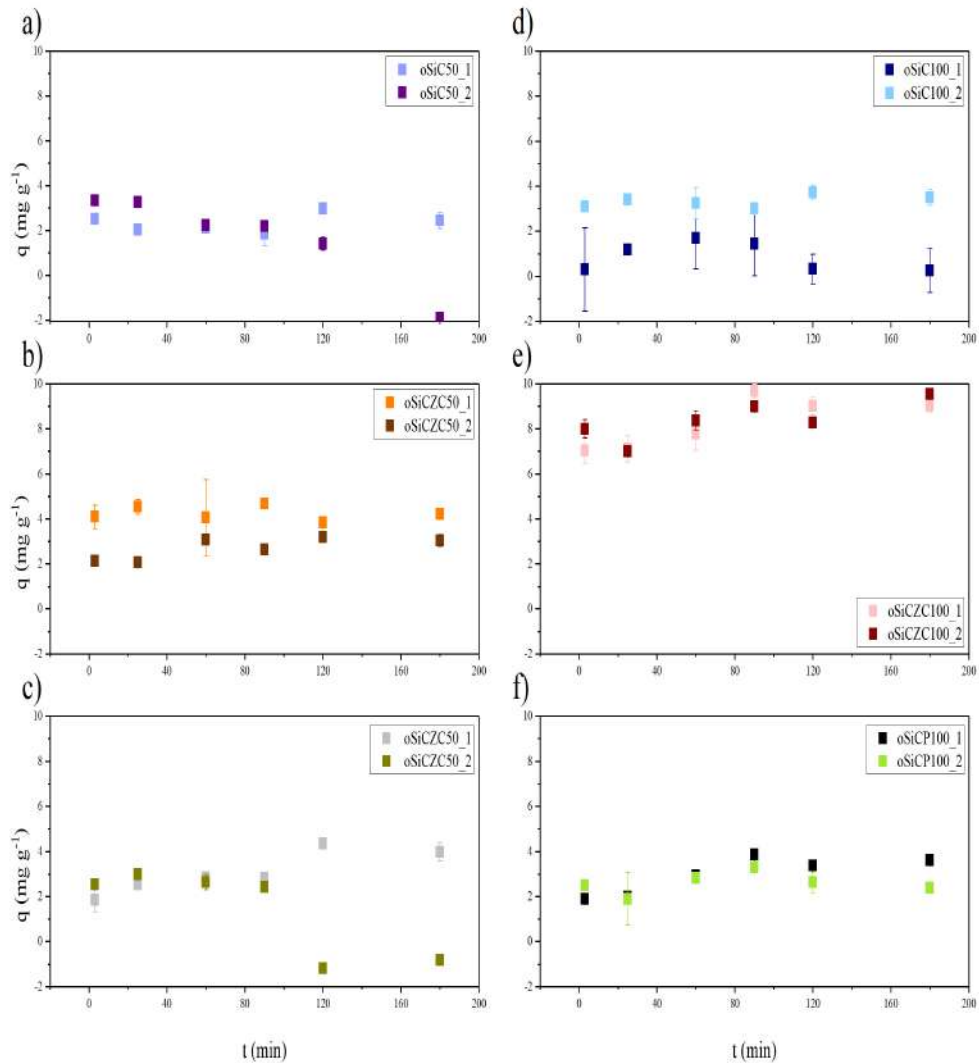
Figure 4.18: Adosption kinetic data for a) oSiC50, b) oSiCZC50, c) oSiCP50, d) oSiC100, e) oSiCZC100, f) oSiCP100.

The kinetic behavior of the data showed a moderately good fitting for the PSO model, specifically for monoliths oSiCZC100 and oSiCP100. This suggest that there is a better chromium (VI) adsorption capacity from metal-functionalized silicon carbide monoliths. The fit was of polynomial nature and did not suit the oSiC50 monoliths. The outcome showcases that the monoliths better fit a kinetic model that implies the chemisorption of chromium (VI) in the material as the type of adsorbate/adsorbent interaction [65, 66].
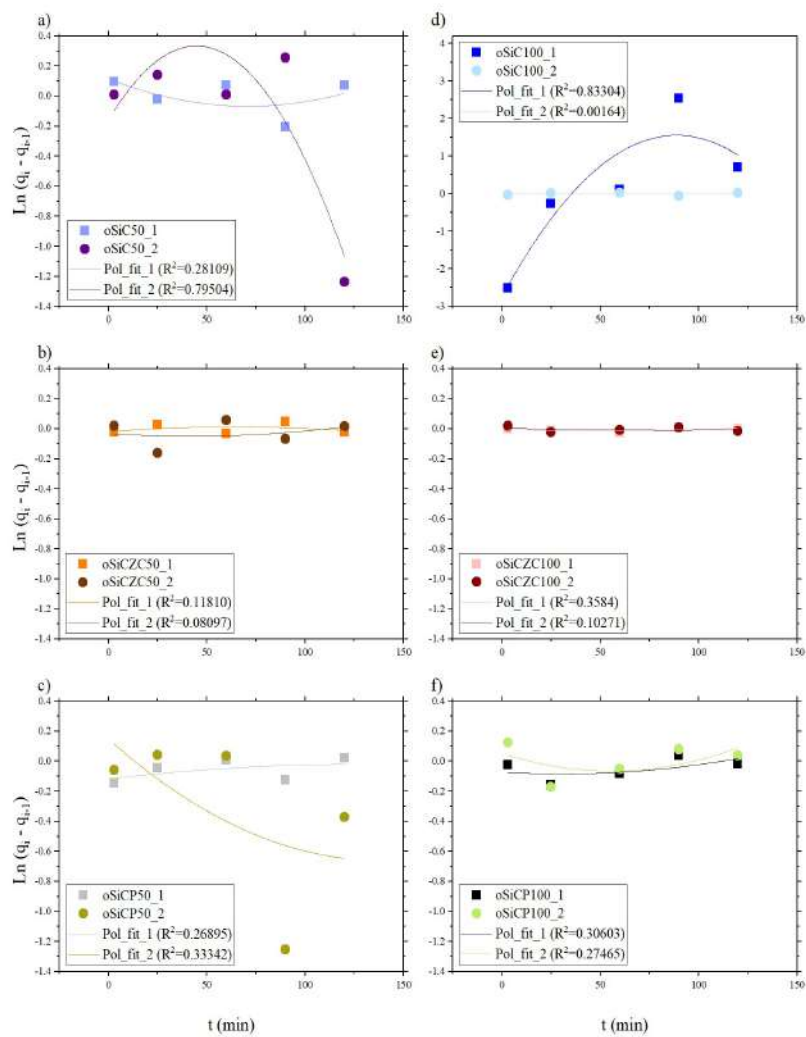
Figure 4.19: PFO model fit to adsorption capacity data.
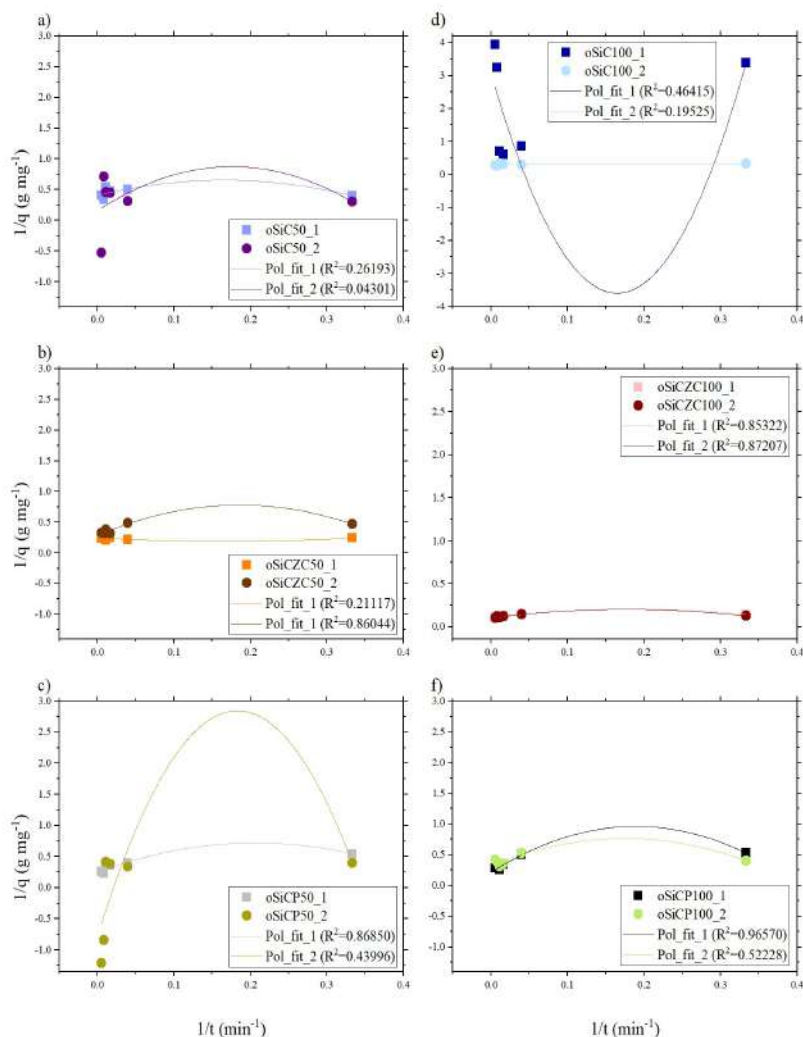
Figure 4.20: PSO model fit to adsorption capacity data.

Photoconversion of 4-nitrophenol (4-NP)

Figure 4.21 and Figure 4.22 depict the catalyst-assisted photodegradation of 4-NP, which showcases a characteristic absorption band at around 317 nm, to 4-aminophenol (4-AP). The left side graphs encompass the experiments performed without $NaBH_4$ while the right side is composed of experiments performed with the reducing agent. The experiments performed without $NaBH_4$ only show the absorption band of 4-NP after the irradiation time (up to 60 min). This is expected as the conversion of this molecule is usually performed

in the presence of excess reducing agent [69].

The experiments performed with $NaBH_4$ show a red shift from the band at 317 nm to 400 nm upon addition of the reducing agent into the acid solution. The appearance of the new band could be caused by the formation of an intermediate compound in the degradation reaction from 4-NP to 4-AP, most likely sodium 4-nitrophenolate (Scheme 1) [69, 86]. Following, there is a decrease in the intensity of the absorption band at 400 nm. This occurs subsequent to the addition of the catalyst (monolith). Thereafter, the behavior of the UV-Vis absorption is not linear with the passing of the time intervals thus, a regression linear fitting is performed to study the impact of the catalyst in the photodegradation reaction. It is worth noting that the reaction performed in the presence of $NaBH_4$ without catalyst (See Figure 6.1 in Chapter 6), the behaviour is analogous and to determine the difference between assisted and non-assisted reaction evolution, this experiment was taking into consideration later in Figure 4.23.
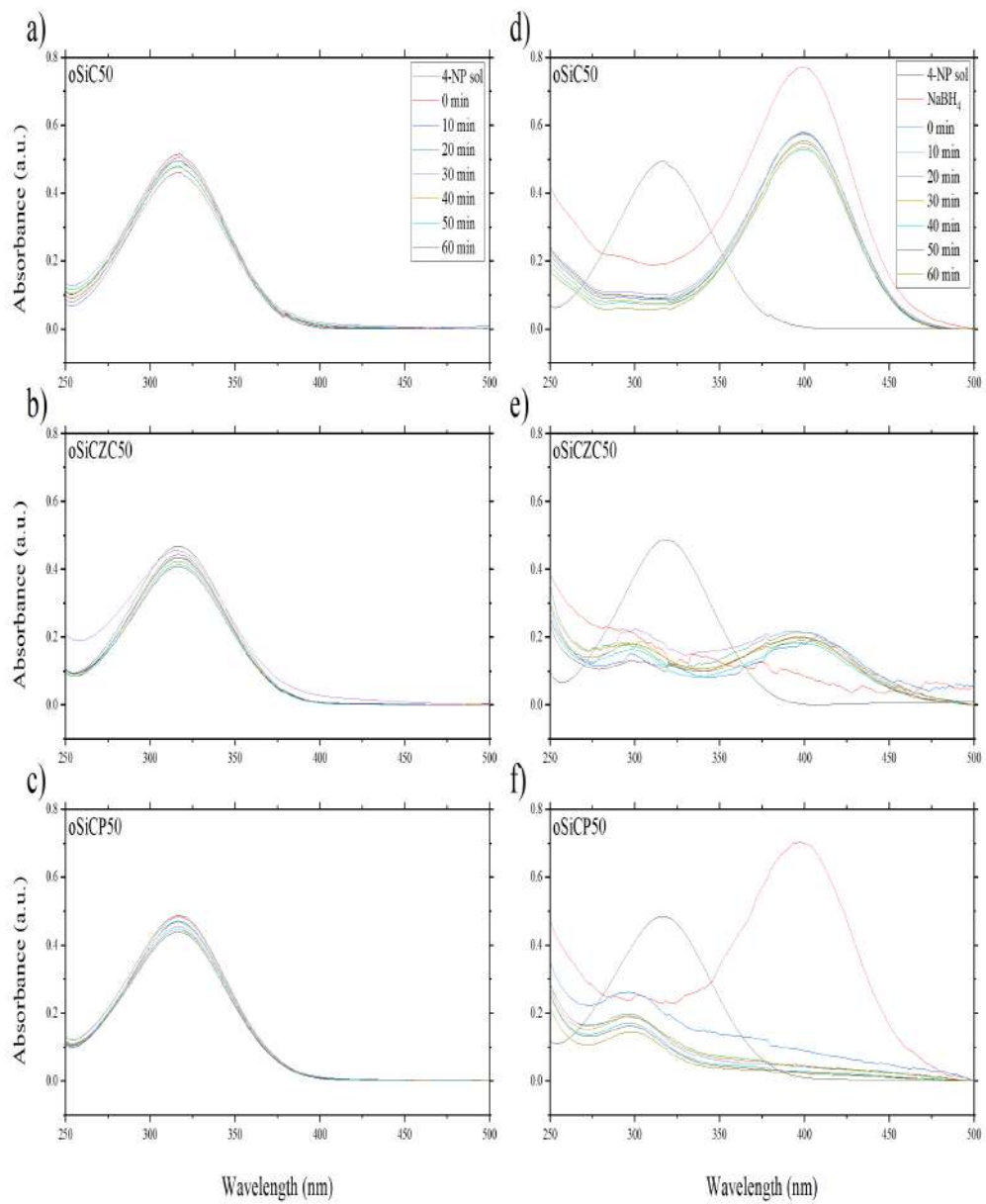
Figure 4.21: UV–Vis spectra of the catalyst-assisted (oSiC50's) photodegradation of 4-NP a-c) without $NaBH_4$ and d-f) in the presence of $NaBH_4$.
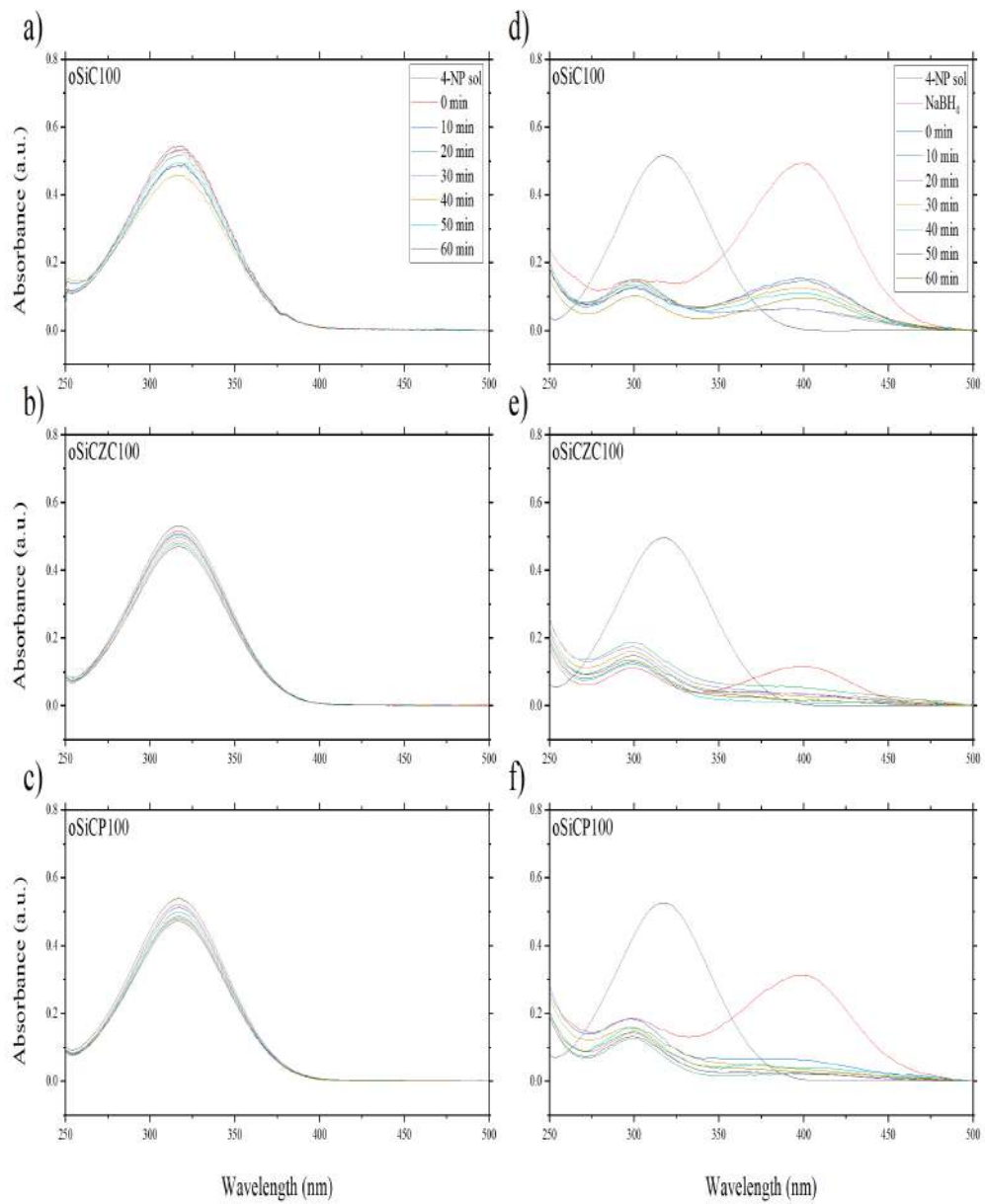
Figure 4.22: UV–Vis spectra of the the catalyst-assisted (oSiC100's) photodegradation of 4-NP a-c) without $NaBH_4$ and d-f) in the presence of $NaBH_4$.

Figure 4.23 represents the fitting for the absorption evolution through time at 400 nm, with and without the addition of SiC catalyst to the acid 4-NP solution. When comparing the R^2 (Coefficient of Determination) values of the various fittings, it is evident that all the values for the catalyst-assisted reaction are closer to 1 than those of the experiments without it. This is a possible indicator that the addition of the catalyst in the 4-NP solution enhances the stability of the reduction reaction compared to that of the non-assisted process.

Furthermore, the best fits for the data are those of oSiCP50 and oSiCZC100, which suggests that said monoliths show the best catalytic performance in the conversion of 4-NP.
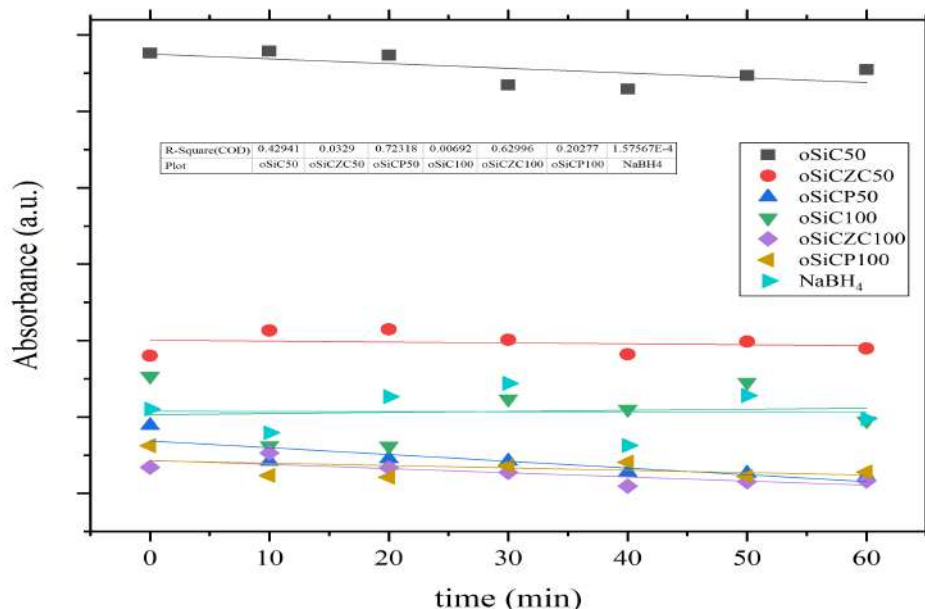
Figure 4.23: Linear fitting model of UV-Vis absorption in the photoreduction of 4-NP at λ=400 nm. Materials employed: oSiC50, oSiCZC50, oSiCP5, oSiC100, oSiCZC100, oSiCP10 and no catalyst.

As seen in the work of Hernandez (2014) [69], the photoreduction of 4-NP was performed in the presence of hydrazine as the reducing agent, with TiO_2 functionalized with silver nanoparticles. The best and most adequate conditions and concentrations for the aforementioned experiment were taking into account for the analogous experiment performed in the present work. Additionally, the positive impact of the catalyst in the photoconversion of 4-NP, as previously stated, implies that the catalyst acts as an intermediate in the hy-

drogen transfer from reducing agent to 4-NP, which indicates the existence of active sites in the catalyst that can adsorb and activate hydrogen species. Therefore, as there was a positive impact in the stability of the reaction, the catalyst (SiC) is a potential catalyst for reactions that entail the production of hydrogen [67, 68].

Chapter 5

Conclusions

5.1 Synthesis Analysis

The appearance of the monoliths synthesized with cyclohexane as the oil phase was vastly different to that of the recycled oil-based monoliths in texture, color and consistency. The cSiC monoliths exhibited a higher level of brittleness and higher amount of cracks along their structure, due to the rapid evaporation of the oil phase. The oSiC monoliths had a significantly different color, due to the orange-ish/ochre color of the raw material; the consistency of them was more viscous, which was evident since the homogenization process, and the resulting material was overall more sturdy and crackless.

When comparing the monoliths with different amount of seed, the best appearance results were from oSiC50, however, the characterization techniques showed a better synthesis outcome for the oSiC100 monoliths.

5.2 Characterization

5.2.1 Composition of SiC

X-ray photoelectron spectroscopy (XPS)

The XPS analysis was succesfull in the elucidation of the obtention of the SiC at a relatively low temperature, which was the main objective of the project. Nevertheless, due to the superficial scope of the chacarterization technique, the elucidation of the metals embedded in the structure of the SiC was not made possible.

The deconvolution of each element encountered in the chemical composition of the material derived in outstanding data fits for the peaks proposed. Consequently it was determined that the material was primarily composed of silicon dioxide, silicon carbide, adventitious carbon and metal oxides.

X-ray Fluorescence (XRF)

The XRF elemental analysis corroborated the presence of metals in the metal-funcionalized monoliths, particularly significant for the ones containing palladium (II). Owing to the fact that the XRF technique verified the presence of metals and not the XPS, which is a surface technique, this proved that the metals are farther embedded in the structure of the material.

Attenuated Total Reflection Fourier Transform Infrared Spectroscopy (ATR-FTIR)

Prior to pyrolysis, the oSiC showed prominent peaks characteristic to the organic raw material employed in the synthesis process. These peaks disappear after the pyrolysis process with the rise of a peak in the region of Si-C, which was attributed to SiC instead of silica due to the XPS results.

The results were similar in the case of all silica monoliths, with the exception of the appearance of carbonaceous residues in oSiC100 monoliths.

5.2.2   Structure of SiC

X-ray Powder Diffraction (XRD)

The XRD analysis of the calcined oSiC monoliths further confirmed the presence of silicon carbide and, to a larger extent, the prevalence of silica (SiO_2). The oSiCP monolith had a more significant degree of crystallinity, made evident from the stronger and more intense peaks displayed in its spectrum.

5.2.3 Applications of SiC

Photoconversion of 4-nitrophenol (4-NP)

The UV-Vis spectra obtained for the evolution of the photodegradation of 4-NP to 4-AP did not evidence the influence of the oSiC monoliths as a catalyst in the reduction reaction in presence of $NaBH_4$. Subsequent to the linear fitting model, it apparent that there was indeed an effect from the catalyst. The improvement was perceived in the stability of the reduction reaction, successfully assisting the reducing agent most commonly employed for 4-NP to 4-AP conversion. In particular, the metal-functionalized monoliths were the ones that provided the better stability to the reaction, in particular the ones with palladium. This discovery could be further studied in applications such as the evolution and production of hydrogen.

Chromium (VI) adsorption evaluation

After the adsorption capacity analysis performed through AAS, the metal-functionalized monoliths were the ones that exhibited the highest chromium (VI) adsorption capacity and as these materials better fitted the PSO model, the interaction between the adsorbate and adsorbent is expected to be chemisorption.

In general:

- It was proved that the synthesis conditions and the employed raw material turned out into β-SiC by the HIPE method.

- It was confirmed that the obtained SiC and the functionalized SiC monoliths have the potential to be used as catalyst for H_2 generation reactions and adsorbent but further work has to be performed.

Bibliography

[1] ChemAxon, "Marvinsketch," 2025, version 24.3.163-demo-site.1. Available at: https://chemaxon.com/products/marvin.

[2] E. Khalife, M. Sabouri, M. Kaveh, and M. Szymanek, "Recent advances in the application of agricultural waste in construction," *Applied Sciences*, vol. 14, no. 6, 2024. [Online]. Available: https://www.mdpi.com/2076-3417/14/6/2355

[3] T. Wang, W. Gong, X. He, Z. Kou, G. Tan, S. Zhou, H. Yu, M. Fan, and H. H. Kung, "Synthesis of highly nanoporous -silicon carbide from corn stover and sandstone," *ACS Sustainable Chemistry & Engineering*, vol. 8, no. 39, pp. 14 896–14 904, 2020. [Online]. Available: https://doi.org/10.1021/acssuschemeng.0c04702

[4] Mohd Sohor, Mohd Aizat Hafiz, Mustapha, Mazli, and Chandra Kurnia, Jundika, "Silicon carbide- from synthesis to application: a review," *MATEC Web Conf.*, vol. 131, p. 04003, 2017. [Online]. Available: https://doi.org/10.1051/matecconf/201713104003

[5] D. M.-C. Chen, B. L. Bodirsky, T. Krueger, A. Mishra, and A. Popp, "The world's growing municipal solid waste: trends and impacts," *Environmental Research Letters*, vol. 15, no. 7, p. 074021, 2020.

[6] N. Gregson and M. Crang, "From waste to resource: The trade in wastes and global recycling economies," *Annual Review of Environment and Resources*, vol. 40, no. Volume 40, 2015, pp. 151–176, 2015. [Online]. Available: https://www.annualreviews.org/content/journals/10.1146/annurev-environ-102014-021105

[7] M. J. Rodríguez-Roque, R. Sánchez-Vega, R. Pérez-Leal, M. C. Soto-Caballero, N. A. Salas-Salazar, and M. A. Flores-Córdova, *By-Products from Oilseed Processing*

and Their Potential Applications. John Wiley Sons, Ltd, 2021, ch. 9, pp. 183–201. [Online]. Available: https://onlinelibrary.wiley.com/doi/abs/10.1002/9781119575313.ch9

[8] R. F. VÃ¡squez-Aguilar and S. GarcÃa Hevia, "Techinical-economic study in avocado cultivation, Atahualpa Canton, El Oro Province," *Revista Ciencias TÃ Agropecuarias*, vol. 30, 09 2021. [Online]. Available: http://scielo.sld.cu/scielo.php?script=sci_arttext&pid=S2071-00542021000300009&nrm=iso

[9] N. D. Shcherban, "Review on synthesis, structure, physical and chemical properties and functional characteristics of porous silicon carbide," *Journal of Industrial and Engineering Chemistry*, vol. 50, pp. 15–28, 2017. [Online]. Available: https://www.sciencedirect.com/science/article/pii/S1226086X17300643

[10] Y. L. Chiew and K. Y. Cheong, "A review on the synthesis of sic from plant-based biomasses," *Materials Science and Engineering: B*, vol. 176, no. 13, pp. 951–964, 2011. [Online]. Available: https://www.sciencedirect.com/science/article/pii/S0921510711002601

[11] A. V. Thulasiraman and M. Ganesapillai, "A systematic review on the synthesis of silicon carbide: An alternative approach to valorisation of residual municipal solid waste," *Processes*, vol. 11, no. 1, 2023. [Online]. Available: https://www.mdpi.com/2227-9717/11/1/283

[12] SoltysL.M., MironyukI.F., MykytynI.M., HnylytsiaI.D., and TurovskaL.V., "Synthesis and properties of silicon carbide (review)," *Physics and Chemistry of Solid State*, vol. 24, no. 1, pp. 5–16, Feb. 2023. [Online]. Available: https://journals.pnu.edu.ua/index.php/pcss/article/view/6226

[13] R. Wu, K. Zhou, C. Y. Yue, J. Wei, and Y. Pan, "Recent progress in synthesis, properties and potential applications of sic nanomaterials," *Progress in Materials Science*, vol. 72, pp. 1–60, 2015. [Online]. Available: https://www.sciencedirect.com/science/article/pii/S0079642515000213

[14] M. Dasog, L. F. Smith, T. K. Purkait, and J. G. C. Veinot, "Low temperature synthesis of silicon carbide nanomaterials using a solid-state method," *Chem. Commun.*, vol. 49, pp. 7004–7006, 2013. [Online]. Available: http://dx.doi.org/10.1039/C3CC43625J

[15] B. Wang, Y. Wang, N. Wu, Y. Gou, C. Han, S. Xie, and D. Fang, "Mesoporous silicon carbide nanofibers with in situ embedded carbon for co-catalyst free photocatalytic hydrogen production," *Nano Research*, vol. 9, 01 2016.

[16] B. Zhao, H. Zhang, H. Tao, Z. Tan, Z. Jiao, and M. Wu, "Low temperature synthesis of mesoporous silicon carbide via magnesiothermic reduction," *Materials Letters*, vol. 65, no. 11, pp. 1552–1555, 2011. [Online]. Available: https://www.sciencedirect.com/science/article/pii/S0167577X11002199

[17] J. Schlichting and F. Riley, "Silicon carbide," in *Concise Encyclopedia of Advanced Ceramic Materials*, R. BROOK, Ed. Oxford: Pergamon, 1991, pp. 426–429. [Online]. Available: https://www.sciencedirect.com/science/article/pii/B9780080347202501179

[18] A. Najafi, F. Golestani-Fard, H. Rezaie, and S. P. Saeb, "Sol-gel synthesis and characterization of sic–b4c nano powder," *Ceramics International*, vol. 47, no. 5, pp. 6376–6387, 2021. [Online]. Available: https://www.sciencedirect.com/science/article/pii/S0272884220332739

[19] S. Sun, L. Song, S. Zhang, H. Sun, and J. Wei, "Pyroelectric hydrogen production performance of silicon carbide," *Ceramics International*, vol. 47, no. 14, pp. 20 486–20 493, 2021.

[20] L. J. C. B, "Formation of silicon carbide from rice hulls," *AMER. CERAM. SOC. BULL.; U.S.A.; DA. 1975; VOL. 54; NO 2; PP. 195-198; BIBL. 10 REF.*, 1975.

[21] J. Su, B. Gao, Z. Chen, J. Fu, W. An, X. Peng, X. Zhang, L. Wang, K. Huo, and P. K. Chu, "Large-scale synthesis and mechanism of -sic nanoparticles from rice husks by low-temperature magnesiothermic reduction," *ACS Sustainable Chemistry & Engineering*, vol. 4, no. 12, pp. 6600–6607, 2016. [Online]. Available: https://doi.org/10.1021/acssuschemeng.6b01483

[22] J. Riikonen, J. Rantanen, R. Thapa, N. T. Le, S. Rigolet, P. Fioux, P. Turhanen, N. K. Bodiford, J. R. Kalluri, T. Ikonen, T. Nissinen, B. Lebeau, J. Vepsäläinen, J. L. Coffer, and V.-P. Lehto, "Rapid synthesis of nanostructured porous silicon carbide from biogenic silica," *Journal of the American Ceramic Society*, vol. 104, no. 2, pp. 766–775, 2021. [Online]. Available: https://ceramics.onlinelibrary.wiley.com/doi/abs/10.1111/jace.17519

[23] M. Xu, Y. R. Girish, K. P. Rakesh, P. Wu, H. M. Manukumar, S. M. Byrappa, Udayabhanu, and K. Byrappa, "Recent advances and challenges in silicon carbide (sic) ceramic nanoarchitectures and their applications," *Materials Today Communications*, vol. 28, p. 102533, 2021. [Online]. Available: https://www.sciencedirect.com/science/article/pii/S2352492821005250

[24] A. A. Mamun, M. McGarrity, J.-H. Kim, and F. Zhao, "Silicon carbide-based dna sensing technologies," *Micromachines*, vol. 14, p. 1557, 08 2023.

[25] S. Rafin, R. Ahmed, M. Haque, M. Hossain, M. Haque, and O. Mohammed, "Power electronics revolutionized: A comprehensive analysis of emerging wide and ultrawide bandgap devices," *Micromachines*, vol. 14, p. 2045, 10 2023.

[26] F. La Via, D. Alquier, F. Giannazzo, T. Kimoto, P. Neudeck, H. Ou, A. Roncaglia, S. E. Saddow, and S. Tudisco, "Emerging sic applications beyond power electronic devices," *Micromachines*, vol. 14, no. 6, p. 1200, 2023.

[27] S. Katiyar and R. Katiyar, "A comprehensive review on synthesis and application of nanocomposites for adsorption of chromium: status and future prospective," *Applied Water Science*, vol. 14, no. 1, dec 2023. [Online]. Available: https://doi.org/10.1007/s13201-023-02062-6

[28] A. Çimen, "Removal of chromium from wastewater by reverse osmosis," *Russian Journal of Physical Chemistry A*, vol. 89, no. 7, pp. 1238–1243, Jul. 2015.

[29] H. Peng and J. Guo, "Removal of chromium from wastewater by membrane filtration, chemical precipitation, ion exchange, adsorption electrocoagulation, electrochemical

reduction, electrodialysis, electrodeionization, photocatalysis and nanotechnology: a review," *Environmental Chemistry Letters*, vol. 18, no. 6, pp. 2055–2068, 2020.

[30] A. Feinle, M. S. Elsaesser, and N. Hüsing, "Sol–gel synthesis of monolithic materials with hierarchical porosity," *Chem. Soc. Rev.*, vol. 45, pp. 3377–3399, 2016. [Online]. Available: http://dx.doi.org/10.1039/C5CS00710K

[31] B. R. Thompson, T. S. Horozov, S. D. Stoyanov, and V. N. Paunov, "Hierarchically structured composites and porous materials from soft templates: fabrication and applications," *J. Mater. Chem. A*, vol. 7, pp. 8030–8049, 2019. [Online]. Available: http://dx.doi.org/10.1039/C8TA09750J

[32] X.-Y. Yang, L.-H. Chen, Y. Li, J. C. Rooke, C. Sanchez, and B.-L. Su, "Hierarchically porous materials: synthesis strategies and structure design," *Chem. Soc. Rev.*, vol. 46, pp. 481–558, 2017. [Online]. Available: http://dx.doi.org/10.1039/C6CS00829A

[33] F. Carn, A. Colin, M.-F. Achard, H. Deleuze, E. Sellier, M. Birot, and R. Backov, "Inorganic monoliths hierarchically textured via concentrated direct emulsion and micellar templates," *J. Mater. Chem.*, vol. 14, pp. 1370–1376, 2004. [Online]. Available: http://dx.doi.org/10.1039/B400984C

[34] J. Hughes, P. Budd, K. Tiede, and J. Lewis, "Polymerized high internal phase emulsion monoliths for the chromatographic separation of engineered nanoparticles," *Journal of Applied Polymer Science*, vol. 132, 07 2014.

[35] N. Cameron and D. Sherrington, "High internal phase emulsions (hipes) - structure, properties and use in polymer preparation," *Advances in Polymer Science*, vol. 126, pp. 162–214, Dec. 1996.

[36] H. Gao, L. Ma, C. Cheng, J. Liu, R. Liang, L. Zou, W. Liu, and D. J. McClements, "Review of recent advances in the preparation, properties, and applications of high internal phase emulsions," *Trends in Food Science Technology*, vol. 112, pp. 36–49, 2021. [Online]. Available: https://www.sciencedirect.com/science/article/pii/S0924224421002338

[37] T. F. Tadros, *Emulsions.* Berlin, Boston: De Gruyter, 2016. [Online]. Available: https://doi.org/10.1515/9783110452242

[38] H. Feng, X. Lu, W. Wang, N.-G. Kang, and J. W. Mays, "Block copolymers: Synthesis, self-assembly, and applications," *Polymers*, vol. 9, no. 10, p. 494, 2017.

[39] Y. Zhao, S.-M. Ma, B. Li, A. De Nicola, N.-S. Yu, and B. Dong, "Micellization of pluronic p123 in water/ethanol/turpentine oil mixed solvents: Hybrid particle–field molecular dynamic simulation," *Polymers*, vol. 11, p. 1806, 11 2019.

[40] P. Ragu, K. Ruparelia, D. A. Venero, and O. T. Mansour, "The characterization of pluronic p123 micelles in the presence of sunscreen agents," *International Journal of Cosmetic Science*, vol. 45, no. 4, pp. 470–479, 2023. [Online]. Available: https://onlinelibrary.wiley.com/doi/abs/10.1111/ics.12856

[41] T. F. Tadros, "Polymeric surfactants," *Principles of Polymer Science and Technology in Cosmetics and Personal Care*, 1999.

[42] A. Sommer-Marquez, C. Mansas, N. Talha, C. Rey, and J. Causse, "Reinforced silica monoliths functionalised with metal hexacyanoferrates for cesium decontamination: a combination of a one-pot procedure and skeleton calcination," *RSC Adv.*, vol. 6, pp. 73 475–73 484, 2016. [Online]. Available: http://dx.doi.org/10.1039/C6RA16980E

[43] P. R. Páramos, J. F. Granjo, M. L. Corazza, and H. A. Matos, "Extraction of high value products from avocado waste biomass," *The Journal of Supercritical Fluids*, vol. 165, p. 104988, 2020. [Online]. Available: https://www.sciencedirect.com/science/article/pii/S0896844620302394

[44] A. E. Sommer Márquez and E. Tapia Maldonado, "Adding value to avocado oil industry wastes: textile wastewater treatment filters made up of activated carbon," August 2021, keywords: Semillas de aguacate, Desperdicios, Aguas residuales, Tintes, Azul de metileno, Adsorción, Avocado seed, Waste, Wastewater, Dye, Methylene-blue, Adsorption. [Online]. Available: http://repositorio.yachaytech.edu.ec/handle/123456789/403

[45] A. E. Sommer Márquez and A. E. Vaca Oviedo, "Encapsulation of photosynthetic plant cells within hierarchical silica monolith enriched with chlorophyll a by high internal phase emulsion (hipe) for co2 adsorption," Feb 2020. [Online]. Available: http://repositorio.yachaytech.edu.ec/handle/123456789/141

[46] A. E. Sommer Márquez, T. Thibault, and A. M. Tipán Quishpe, "Possibility of reusing industrial waste to synthesize a depolluting silica monolith through hipe method: an experimental and theoretical study," Oct 2020. [Online]. Available: http://repositorio.yachaytech.edu.ec/handle/123456789/230

[47] A. E. Sommer Márquez and N. P. López Pico, "Algae encapsulation into silica monoliths synthesized by high internal phase emulsions (hipe)," Feb 2020. [Online]. Available: http://repositorio.yachaytech.edu.ec/handle/123456789/191

[48] A. E. Sommer Márquez and D. B. Terán Arellano, "Environmental water depollution by using hierarchically textured hybrids algae-silica monoliths," Aug 2021. [Online]. Available: http://repositorio.yachaytech.edu.ec/handle/123456789/416

[49] A. E. Sommer Márquez and C. V. Cervantes Burbano, "Increasing of photochemical activity of bioentities by the combination of algae and grass-chloroplasts when encapsulated into hierarchical silica-monoliths," Jul 2022. [Online]. Available: http://repositorio.yachaytech.edu.ec/handle/123456789/535

[50] A. E. Sommer Márquez and K. F. Montesdeoca Arredondo, "Using mining industry wastewater to obtain prussian blue analogues-silica monolith hybrids: a key to reduce water pollution," Jan 2022. [Online]. Available: http://repositorio.yachaytech.edu.ec/handle/123456789/491

[51] A. Vaca-Oviedo, J. Causse, and A. Sommer-Márquez, "Immobilization of chloroplasts from grass within a silica matrix synthetized by hipe method," *MRS Advances*, vol. 5, no. 14–15, p. 727–733, 2020.

[52] A. Sommer, "Retención de clorofila en hidrotalcitas," 2013.

[53] I. Thushari and S. Babel, "Comparative study of the environmental impacts of used cooking oil valorization options in thailand," *Journal of Environmental Management*, vol. 310, p. 114810, 2022.

[54] W. H. Foo, S. S. N. Koay, S. R. Chia, W. Y. Chia, D. Y. Y. Tang, S. Nomanbhay, and K. W. Chew, "Recent advances in the conversion of waste cooking oil into value-added products: A review," *Fuel*, vol. 324, p. 124539, 2022.

[55] PROGEDEON, "Progedeon official website," 2024. [Online]. Available: https://www.progedeon.com/

[56] El Universo, "Reciclar 140 toneladas de aceite usado de cocina al mes en ecuador es nueva meta de iniciativa de empresa privada," 2021. [Online]. Available: https://www.eluniverso.com/noticias/economia/reciclar-140-toneladas-de-aceite-usado-de-cocina-al-mes-en-ecuador-es-nueva-meta-de-iniciativa

[57] J. P. Blitz, "Diffuse reflectance spectroscopy," pp. 185–219, 1998.

[58] P. em. Dr. Heinz-Helmut Perkampus, "Uv-vis spectroscopy and its applications," in *Springer Lab Manuals*, 1992. [Online]. Available: https://api.semanticscholar.org/CorpusID:3247263

[59] D. K. Singh, M. Pradhan, and A. Materny, *Modern Techniques of Spectroscopy*. Springer, 2021.

[60] J. Epp, "4 - x-ray diffraction (xrd) techniques for materials characterization," in *Materials Characterization Using Nondestructive Evaluation (NDE) Methods*, G. Hübschen, I. Altpeter, R. Tschuncky, and H.-G. Herrmann, Eds. Woodhead Publishing, 2016, pp. 81–124. [Online]. Available: https://www.sciencedirect.com/science/article/pii/B9780081000403000043

[61] J. F. Moulder, W. F. Stickle, W. M. Sobol, and K. D. Bomben, "Handbook of x-ray photoelectron spectroscopy," in *Handbook of X-Ray Photoelectron Spectroscopy*, 1992. [Online]. Available: https://api.semanticscholar.org/CorpusID:133719866

[62] B. Beckhoff, B. Kanngießer, N. Langhoff, R. Wedell, and H. Wolff, *Handbook of practical X-ray fluorescence analysis.* Springer Science & Business Media, 2007.

[63] B. Welz and M. Sperling, *Atomic Absorption Spectrometry.* Wiley, 2008. [Online]. Available: https://books.google.com.ec/books?id=xSV5hkuI5l8C

[64] L. M. De Lima Eljuri and D. S. Peñaloza Tinoco, "Synthesis and characterization of chitosan aerogels for removal of cr(vi) from wastewater," jun 2023. [Online]. Available: http://repositorio.yachaytech.edu.ec/handle/123456789/626

[65] J. C. Bullen, S. Saleesongsom, K. Gallagher, and D. J. Weiss, "A revised pseudo-second-order kinetic model for adsorption, sensitive to changes in adsorbate and adsorbent concentrations," *Langmuir*, vol. 37, no. 10, pp. 3189–3201, 2021.

[66] M. Musah, Y. Azeh, J. T. Mathew, M. T. Umar, Z. Abdulhamid, and A. I. Muhammad, "Adsorption kinetics and isotherm models: a review," *CaJoST*, vol. 4, no. 1, pp. 20–26, 2022.

[67] K. Maeda, "Photocatalytic water splitting using semiconductor particles: History and recent developments," *Journal of Photochemistry and Photobiology C: Photochemistry Reviews*, vol. 12, no. 4, pp. 237–268, 2011. [Online]. Available: https://www.sciencedirect.com/science/article/pii/S1389556711000505

[68] A. Naldoni, M. Altomare, G. Zoppellaro, N. Liu, Kment, R. Zbořil, and P. Schmuki, "Photocatalysis with reduced tio2: From black tio2 to cocatalyst-free hydrogen production," *ACS Catalysis*, vol. 9, no. 1, pp. 345–364, 2019, pMID: 30701123. [Online]. Available: https://doi.org/10.1021/acscatal.8b04068

[69] A. Hernández-Gordillo, M. Arroyo, R. Zanella, and V. Rodríguez-González, "Photo-conversion of 4-nitrophenol in the presence of hydrazine with agnps-tio2 nanoparticles prepared by the sol–gel method," *Journal of hazardous materials*, vol. 268, pp. 84–91, 2014.

[70] L. Díaz-Muñoz, A. Bonilla-Petriciolet, H. Reynel-Ávila, and D. Mendoza-Castillo, "Sorption of heavy metal ions from aqueous solution using acid-treated

avocado kernel seeds and its ftir spectroscopy characterization," *Journal of Molecular Liquids*, vol. 215, pp. 555–564, 2016. [Online]. Available: https://www.sciencedirect.com/science/article/pii/S0167732215306802

[71] A. Rahmat and M. Apriyanto, "Evaluation of the characteristics of avocado seed biochar at various pyrolysis temperatures for sustainable waste management," *Universal Journal of Agricultural Research*, 2024.

[72] E. Barbosa-Martín, L. Chel-Guerrero, E. González-Mondragón, and D. Betancur-Ancona, "Chemical and technological properties of avocado (persea americana mill.) seed fibrous residues," *Food and Bioproducts processing*, vol. 100, pp. 457–463, 2016.

[73] S. Martins, K. V. Pontes, R. Fialho, and F. Fakhouri, "Extraction and characterization of the starch present in the avocado seed (persea americana mill) for future applications," *Journal of Agriculture and Food Research*, vol. 8, p. 100303, 2022.

[74] A. A. A. Wahab, S. H. Chang, and A. Som, "Characterization of waste cooking oil as a potential green solvent for liquid-liquid extraction," in *International Conference on Advances in Civil and Environmental Engineering*, vol. 2015, 2015, pp. 20–28.

[75] R. A. Nyquist, *Interpreting infrared, Raman, and nuclear magnetic resonance spectra.* Academic Press, 2001, vol. 2.

[76] Z. Luo, C. Wan, H. Xu, F. Zhao, and Z. Jin, "Effect of pulsed uv laser irradiation on 4h-sic mos with thermal gate oxide," *Journal of Materials Science: Materials in Electronics*, vol. 31, pp. 5838–5842, 2020.

[77] T. F. Scientific. (n.d.) Carbon. [Online]. Available: https://www.thermofisher.com/ec/en/home/materials-science/learning-center/periodic-table/non-metal/carbon.html

[78] X. Fitting. (n.d.) Carbon. [Online]. Available: https://www.xpsfitting.com/search/label/carbon

[79] N. I. of Standards and T. (NIST). (n.d.) Xps spectra identifier. [Online]. Available: https://srdata.nist.gov/xps/SpectraIdentifier

[80] T. F. Scientific. (n.d.) Oxygen. Accessed: 2024-08-11. [Online]. Available: https://www.thermofisher.com/ec/en/home/materials-science/learning-center/periodic-table/non-metal/oxygen.html

[81] ——. (n.d.) Silicon. [Online]. Available: https://www.thermofisher.com/ec/en/home/materials-science/learning-center/periodic-table/metalloid/silicon.html

[82] K. Teker and D. Abdurazik, "Single source fabrication of sic nanowires and ftir spectroscopy," *Journal of Optoelectronics and Advanced Materials*, vol. 18, 2016.

[83] K. Sun, T. Wang, Z. Chen, W. Lu, X. He, W. Gong, M. Tang, F. Liu, Z. Huang, J. Tang *et al.*, "Clean and low-cost synthesis of high purity beta-silicon carbide with carbon fiber production residual and a sandstone," *Journal of Cleaner Production*, vol. 238, p. 117875, 2019.

[84] J. Ding, C. Deng, W. Yuan, H. Zhu, and X. Zhang, "Novel synthesis and characterization of silicon carbide nanowires on graphite flakes," *Ceramics International*, vol. 40, no. 3, pp. 4001–4007, 2014.

[85] N. Mayedwa, N. Mongwaketsi, S. Khamlich, K. Kaviyarasu, N. Matinise, and M. Maaza, "Green synthesis of nickel oxide, palladium and palladium oxide synthesized via aspalathus linearis natural extracts: physical properties & mechanism of formation," *Applied Surface Science*, vol. 446, pp. 266–272, 2018.

[86] D. Al-Namil, E. Khoury, and D. Patra, "Solid-state green synthesis of ag nps: Higher temperature harvests larger ag nps but smaller size has better catalytic reduction reaction," *Scientific Reports*, vol. 9, p. 15212, 2019.

Appendices

Chapter 6

Appendix A

Table 6.1: XRF organic analysis of oSiC50

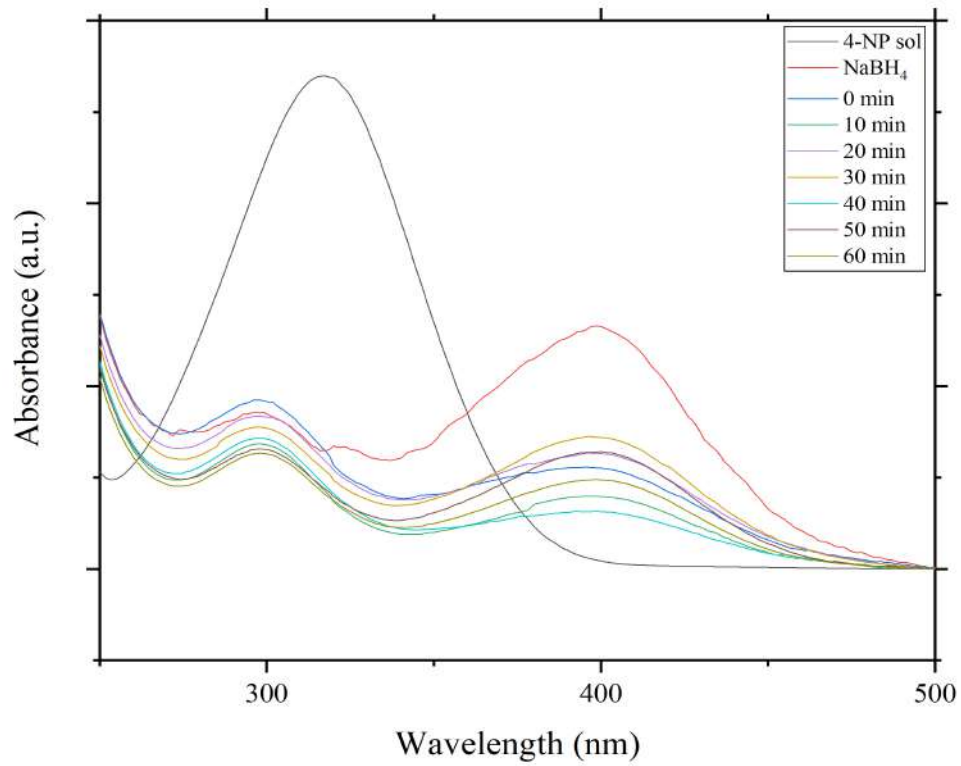| Element	Concentration (%) oSiC50
Si	11.030
Al	0.018
Fe	0.032
CH_2	88.737
Ca	0.096
P	0.065
K	0.012
S	0.005
Cr	0.004
Cu	0.001
Ni	0.001

Figure 6.1: UV-Vis spectrum of the photodegradation of 4-NP in the presence of $NaBH_4$ without catalyst.
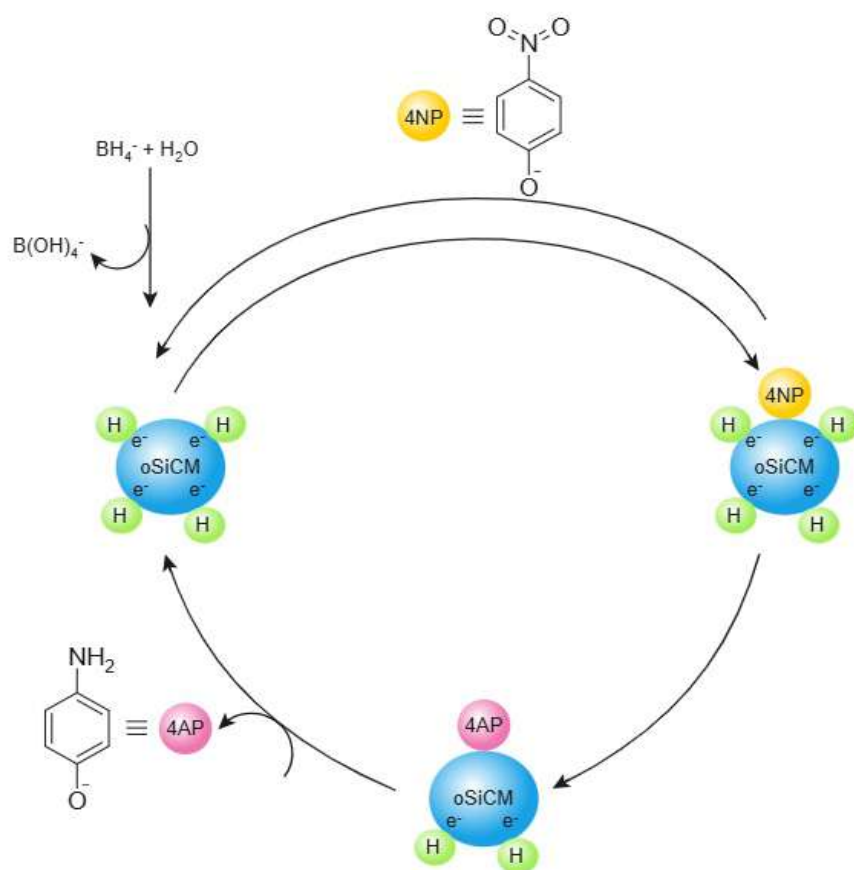
Figure 6.2: Proposed reaction mechanism for the catalyst-assisted photoreduction of 4NP. Scheme created using MarvinSketch (ChemAxon, version 24.3.163-demo-site.1) [1].